Shape of atomic nuclei in heavy ion collisions

Jiangyong Jia ⊙*

Department of Chemistry, Stony Brook University, Stony Brook, New York 11794, USA
and Physics Department, Brookhaven National Laboratory, Upton, New York 11976, USA

In the hydrodynamic model description of heavy ion collisions, the final-state anisotropic flows v_n are linearly related to the strengths of the multipole shape of the distribution of nucleons in the transverse plane, ε_n: $v_n \propto \varepsilon_n$. The ε_n, for $n = 1, 2, 3, 4$, are sensitive to the shapes of the colliding ions, characterized by the quadrupole β_2, octupole β_3, and hexadecapole β_4 deformations. This sensitivity is investigated analytically and also in a Monte Carlo Glauber model. One observes a robust linear relation, $\langle \varepsilon_n^2 \rangle = a'_n + b'_n \beta_n^2$, for events in a fixed centrality. The $\langle \varepsilon_2^2 \rangle$ has a contribution from β_3 and β_4, and $\langle \varepsilon_3^2 \rangle$ from β_4. In ultracentral collisions, there are little cross contributions between β_2 and ε_3 and between β_3 and ε_2, but clear cross contributions are present in noncentral collisions. Additionally, $\langle \varepsilon_n^2 \rangle$ are insensitive to nonaxial shape parameters such as the triaxiality. This is good news because the measurements of v_2, v_3, and v_4 can be used to constrain simultaneously the β_2, β_3, and β_4 values. This is best done by comparing two colliding ions with similar mass numbers and therefore nearly identical a'_n, to obtain a simple equation that relates the β_n of the two species. This opens up the possibility to map the shape of the atomic nuclei at a timescale ($< 10^{-24}$ s) much shorter than probed by low-energy nuclear structure physics ($< 10^{-21}$ s), which ultimately may provide information complementary to that obtained in the nuclear structure experiments.

I. INTRODUCTION

Most atomic nuclei in their ground state are deformed from a well defined spherical shape. The deformation has nontrivial dependence on the proton and neutron numbers, especially in the vicinity of a full shell or subshell, reflecting collective motion induced by interaction between valence nucleons and shell structure [1]. The collective motion leads to characteristic rotational spectra of nuclear excited state, where the electric multipole transition probability $B(En)$ between low-lying rotational states with $n\hbar$ difference in angular momentum can be used to infer the shape parameters. Past efforts have led to the discovery of a rich variety of phenomena, such as quadrupole deformation, shape evolution, triaxiality/shape coexistence, octupole deformation, hexadecapole deformation, and other exotic shapes [2–6].

No one has directly observed the deformed nucleus, however. This is because the nucleus is deformed in the so-called intrinsic (body-fixed) frame, and its wave function in the laboratory frame actually does not pick a particular direction. Typical scattering experiments probe the nuclear form factors averaged over all orientations, and the static deformation appears mostly as an increased surface thickness [7]. On the other hand, high-energy heavy ion collisions at the BNL Relativistic Heavy Ion Collider (RHIC) and the CERN Large Hadron Collider (LHC), as illustrated in Fig. 1, can image the shapes of nuclei by colliding them together and looking at the collective expansion of the produced system cor-

responding to the geometry of the overlap. In these collisions, two Lorentz-contracted nuclei, by a factor of 100 at RHIC and more than a factor of 1000 at the LHC, cross each other over a timescale $\tau < 0.1$ fm/$c \approx 3 \times 10^{-24}$ s, forming a hot and dense quark-gluon plasma (QGP) [8] in the overlap region, whose initial shape is correlated with the deformed shape of the nuclei. Driven by the large pressure gradient forces, the QGP expands hydrodynamically, converting the spatial anisotropies into azimuthal anisotropies of final-state particles in the momentum space [9]. Nuclear shape imaging is possible because each collision probes simultaneously the entire mass distribution of the nuclei, and one can use particle correlations among thousands of produced particles to infer the two-point and multipoint correlations of this mass distribution and hence its spatial shape. Since the timescales involved in these collisions are much shorter ($< 10^{-24}$ s) than the typical timescale of the rotational bands (10^{-21} s [10]), this raises an important question of whether the manifestation of nuclear deformation—a collective feature of the nuclear many-body system—is the same across energy scales [11].

The shape of the nucleus in nuclear physics is often modeled though a nucleon density profile of the Woods-Saxon form,

$$\rho(r, \theta, \phi) = \frac{\rho_0}{1 + e^{[r - R(\theta, \phi)/a_0]}},$$

$$R(\theta, \phi) = R_0 \bigg(1 + \beta_2 [\cos\gamma\, Y_{2,0} + \sin\gamma\, Y_{2,2}]$$

$$+ \beta_3 \sum_{m=-3}^{3} \alpha_{3,m} Y_{3,m} + \beta_4 \sum_{m=-4}^{4} \alpha_{4,m} Y_{4,m} \bigg), \quad (1)$$

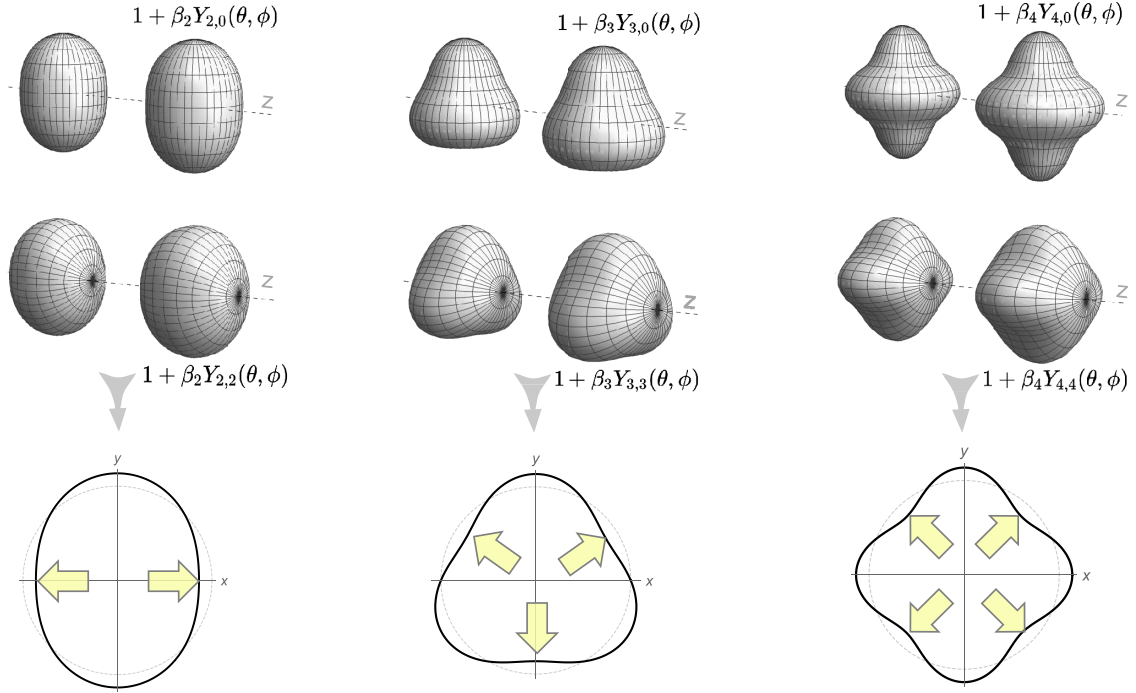*Corresponding author: jiangyong.jia@stonybrook.edu

FIG. 1. A diagram of the collision of nuclei with quadrupole (left), octupole (middle), and hexadecapole (right) deformations including either the $Y_{n,0}$ mode (top row) or the $Y_{n,n}$ mode (middle row) and with $\beta_n = 0.25$. The Lorentz contractions in the z direction, by factor of 100 at RHIC and more than a factor of 1000 at the LHC, are not shown. The bottom row represents the initial conditions of the QGP formed after the collision in the transverse plane. The hollow arrows indicate the direction of maximum pressure gradients along which the medium expands with largest velocity, leading to final state harmonic flow v_n with n-fold symmetry.

where the nuclear surface $R(\theta, \phi)$ is expanded in spherical harmonics $Y_{n,m}$, but keeping only the terms that are most relevant in nuclear structure physics, i.e., quadrupole $n = 2$, octupole $n = 3$, and hexadecapole $n = 4$. Note that the $Y_{2,-1}$, $Y_{2,1}$, and $Y_{2,-2}$ are used to define the intrinsic frame, leaving $Y_{2,0}$ and $Y_{2,2}$ as the only relevant quadrupole components (higher order deformations defined in this frame should have all components as relevant degrees of freedom). The positive number β_2 describes the overall quadrupole deformation, and the triaxiality parameter γ controls the relative order of the three radii R_a, R_b, R_c of the nucleus in the intrinsic frame. It has the range $0 \leqslant \gamma \leqslant \pi/3$, with $\gamma = 0$, $\gamma = \pi/3$, and $\gamma = \pi/6$ corresponding, respectively, to prolate $(R_a = R_b < R_c)$, oblate $(R_a < R_b = R_c)$ or maximum triaxiality $(R_a < R_b < R_c$ and $2R_b = R_a + R_c)$. Similarly, β_3 and β_4 control the overall octupole and hexadecapole deformations, respectively. The $\alpha_{3,m}$ and $\alpha_{4,m}$, in analogy to γ, are internal "angular" parameters describing deviation from axial and/or reflection symmetry, and they satisfy the normalization conditions $\sum_{m=-3}^{3} \alpha_{3m}^2 = 1$ and $\sum_{m=-4}^{4} \alpha_{4m}^2 = 1$.

In heavy ion collisions, the initial condition and dynamics of QGP are naturally formulated in a cylindrical coordinate system with the z axis coinciding with the beam line. The initial condition is determined by the distribution of nucleons in the transverse plane $\rho(r_\perp, \phi)$, which drives the collective flow of final-state particles, reflected by the momentum spectrum $N(p_T, \phi)$. $N(p_T, \phi)$ is often analyzed in terms of a Fourier expansion, $dN/d\phi \propto 1 + 2 \sum_n v_n(p_T) \cos n[\phi - \Psi_n(p_T)]$. The $\rho(r_\perp, \phi)$ is fully characterized via a two-dimensional 2D

multipole expansion, whose leading radial modes have the following expression [12,13] in the center-of-mass frame:

$$\varepsilon_1 e^{i\Phi_1} = - \int d^2 r_\perp r_\perp^3 e^{i\phi} \rho(\vec{r}_\perp) \Big/ \int d^2 r_\perp r_\perp^3 \rho(\vec{r}_\perp),$$

$$\varepsilon_n e^{in\Phi_n}|_{n>1} = - \int d^2 r_\perp r_\perp^n e^{in\phi} \rho(\vec{r}_\perp) \Big/ \int d^2 r_\perp r_\perp^n \rho(\vec{r}_\perp). \tag{2}$$

The 2D eccentricity vectors $\varepsilon_n e^{in\Phi_n}$ are a close analog of $Y_{n,m}$ in the 3D case. In fact, the eccentricity vectors for $n > 1$ are directly related to the multipole moments of the mass distribution, $\varepsilon_n e^{in\Phi_n} \propto -\langle Y_n^n \rangle$, which I will show later lead to a simple relation between ε_n and β_n. Note that the radial weight of ε_1 is $r_\perp^3$ instead of the naively expected $r_\perp$, because the latter contribution vanishes in the center-of-mass frame and $r_\perp^3$ weighting gives the next radial mode.

Study of the relation between the initial-state ε_n and final-state v_n, within the relativistic viscous hydrodynamics or transport model framework, has always been a central focus of the heavy ion community. Comprehensive model and data comparisons [14] show very good linear relations, $v_n = k_n \varepsilon_n$, not only on average but also for each event,[1] where the response coefficients k_n capture the transport properties of the QGP produced in the collision. Thanks to the precision

---

[1]The linear relation is very good for $n = 2$ and 3 in general and for $n = 1$ and $n = 4$ in the case of central collisions [15].

measurements of v_n and its event-by-event fluctuations $p(v_n)$ [8,16], and detailed understanding of the properties of k_n [15,17–19], hydrodynamic models can now determine the ε_n and $p(\varepsilon_n)$ with enough precision to constrain the deformation parameters.

Influence of nuclear deformation on dynamics of heavy ion collisions was considered early on [20–22]. More recent studies focused on the relation between β_2 and v_2 [23–28]. Experimental evidence for quadrupole deformation appear as large differences of v_2 between ultracentral collisions (UCC) of different systems, in particular between $^{197}\mathrm{Au} + ^{197}\mathrm{Au}$ and $^{238}\mathrm{U} + ^{238}\mathrm{U}$ collisions at RHIC [29] and between $^{129}\mathrm{Xe} + ^{129}\mathrm{Xe}$ and $^{208}\mathrm{Pb} + ^{208}\mathrm{Pb}$ collisions at the LHC [30–32]. Reference [11] explored the parametric dependence of various flow observables on β_2, and find that both ϵ_2^2 and v_2^2 depend linearly on β_2^2; a simple formula is derived relating the β_2 in the two collision systems to the ratio of v_2. The influence of octupole deformation is considered recently in Pb + Pb collisions to explain the order of v_2 and v_3 in the UCC region [33].

Another observable showing a strong sensitivity to the nuclear deformation is the Pearson correlation coefficient, $\rho(v_2^2, [p_T])$, between v_2 and the mean transverse momentum, $[p_T]$, which probes both the β_2 [34,35] and its triaxiality γ [36] of the colliding ions. Recent measurement from the STAR Collaboration [37] established unambiguously the large and dominating influence of the nuclear quadrupole deformation of $^{238}\mathrm{U}$. The large prolate deformation of $^{238}\mathrm{U}$ yields a strong negative contribution to the $\rho(v_2^2, [p_T])$, enough to make it change sign. Large influence of deformation is also observed in the fluctuations of $[p_T]$ [37].

Continuing this line of work, I explore the parametric dependence of ϵ_1, ϵ_2, ϵ_3, and ϵ_4 on various deformation parameters β_n and deviations from axial and reflection symmetries [γ and combinations of $\alpha_{n,m}$ in Eq. (1)]. In the UCC region, the mean square (ms) values of ϵ_n, $\langle \epsilon_n^2 \rangle$, are found to be driven primarily by β_n of the same order, and the triaxiality parameter γ only has very modest impact on ϵ_2. Away from the UCC region, $\langle \epsilon_n^2 \rangle$ are insensitive to γ, but they receive contributions from β_m of a different order $m \neq n$. In other words, I establish the following empirical relation:

$$\langle \epsilon_n^2 \rangle = a'_n + b'_n \beta_n^2 + \sum_{m \neq n} b'_{n,m} \beta_m^2,$$

$$n = 1, 2, 3, 4, \ m = 2, 3, 4 \text{ and } b'_1 = 0, \qquad (3)$$

with significant values of $b'_{n,m}$ observed for $b'_{1,3}$, $b'_{1,4}$, and $b'_{3,4}$. Since $v_n \propto \epsilon_n$, one expects similar parametric dependencies to hold between $\langle v_n^2 \rangle$ and β_m. This simple scaling relation provides a strong motivation for a collision system scan to map out the shape of atomic nuclei in the most interesting region of nuclear chart and compare with the knowledge from nuclear structure physics.

II. ANALYTICAL ESTIMATE IN ULTRACENTRAL COLLISIONS AND GLAUBER MODEL SETUP

To gain some intuitive insight on Eq. (3) it is useful to demonstrate its validity using a simpler version of the nu-

clear surface. Here I consider a density distribution of the liquid-drop model with a sharp surface, $\rho(r, \theta, \phi) = \rho_0$ when $r < R(\theta, \phi)$ and zero otherwise, and I assume that the energy density distribution is given by the distribution of participating nucleons. I limit the discussion to head-on collisions with nearly maximum overlap; i.e.; the two nuclei not only have zero impact parameter, but are also required to align in a way to ensure the overlap region contains all the nucleons $N_{\mathrm{part}} = 2A$. In reality, the selection of UCC events naturally encompasses a wider range of rotation angles and also a finite range of N_{part}, therefore I also study a second case which requires zero impact parameter but independent rotations for the two nuclei. The details of the calculation can be found in Appendix A.

As illustrated in Fig. 1, the maximum ε_n for $Y_{n,0}$ is reached in a "body-body" configuration, when the symmetry axis of the nuclei is perpendicular to the beam. In the case of $Y_{n,n}$, the maximum ε_n is reached in a "tip-tip" configuration, when the z axis of the nuclei is aligned with the beam. For these two configurations, it is straightforward to calculate eccentricities: they are listed in the first two rows of Table I. However, one is more interested in the eccentricity values averaged over random orientations. The first nontrivial and the most important moment is $\langle \varepsilon_n^2 \rangle$, which relates directly to the $\langle v_n^2 \rangle$ measured by the two-particle correlation method. The results obtained by requiring same random rotations for the two nuclei are listed in the third row of Table I, and those obtained by requiring independent random rotations the two nuclei are listed in the last row of Table I. The two cases have the same dependencies but the coefficients are a factor of 2 smaller in the second case.

A few remarks are in order. The maximum possible ε_n values are different between $Y_{n,n}$ and $Y_{n,0}$, and they are generally comparable to the corresponding β_n value. However, the ms values after averaging over random orientations have exactly the same quadratic dependence on β_n, showing no explicit dependence on the internal angular variables γ and $\alpha_{n,m}$ in Eq. (1) to the leading order.[2] Remarkably, the octupole deformation also gives rise to a dipolar eccentricity, following the same quadratic dependence on β_3 but with a coefficient that is a factor of 10 smaller. Furthermore, the quadrupole deformation gives rise to a quartic contribution to ε_4, and, in an analogy to the well-known non-inear contribution of ε_2 to ε_4 [13], scales as $\langle \varepsilon_4^2 \rangle \approx (0.7–1.4)\langle \varepsilon_2^2 \rangle^2$. Lastly, the coefficients $b'_{n,m}$ listed in the table are derived under a simplified scenario. In a more realistic Monte Carlo Glauber model calculation based on the Woods-Saxon nuclear profile, the coefficients in the UCC region as shown in bottom row of Fig. 2 are comparable to or slightly smaller than those obtained by requiring zero impact parameter and independent rotations.

For a more realistic estimation of influence of nuclear deformation, a Monte Carlo Glauber model [38] is used to simulate collisions of $^{238}\mathrm{U}$ and $^{96}\mathrm{Zr}$ systems and calculate ε_n in each event. These systems are chosen because the experimental collision data exist already. The nucleons are

---

[2]The actual probability density distribution $p(\varepsilon_n)$ is different between deformations described by $Y_{n,n}$ and by $Y_{n,0}$. This difference can be captured by the fourth- and higher-order cumulants.

TABLE I. The value of eccentricity generated by the deformation component $Y_{n,0}$ (first row) and $Y_{n,n}$ (second row) for the special alignment of two colliding nuclei similar to those shown in Fig. 1 which maximizes the eccentricity values, obtained within an optical Glauber model with sharp surface by setting $a_0 = 0$ in Eq. (1). Here only the leading- and subleading-order contributions are included. The leading-order mean-square values $\langle \varepsilon_n^2 \rangle$ obtained by averaging over common random orientations for the two nuclei and independent random orientations for the two nuclei are given in the third row and the last row, respectively. The values in the latter case are a factor of 2 smaller, but in both cases they are independent of γ, $\alpha_{3,m}$, or $\alpha_{4,m}$.

	$n=1$	$n=2$	$n=3$	$n=4$
$1 + \sum_{m=2}^4 \beta_m Y_{m,0}$ ε_n (body-body)	$\frac{16}{5\pi\sqrt{7\pi}}\beta_3$ $+\frac{302}{3\sqrt{35}\pi^2}\beta_2\beta_3+\frac{493967\sqrt{7}}{73920\pi^2}\beta_3\beta_4$ $=0.22\beta_3$ $+1.7\beta_2\beta_3+1.8\beta_3\beta_4$	$\sqrt{\frac{45}{16\pi}}\beta_2+\frac{15}{112\pi}\beta_2^2$ $+\frac{9\sqrt{5}}{7\pi}\beta_2\beta_4+\frac{75}{77\pi}\beta_4^2+\frac{1}{\pi}\beta_3^2$ $=0.95\beta_2+0.043\beta_2^2$ $+0.92\beta_2\beta_4+0.31\beta_4^2+0.32\beta_3^2$	$\frac{16}{\pi\sqrt{7\pi}}\beta_3$ $+\frac{2\sqrt{35}}{3\pi^2}\beta_2\beta_3+\frac{2067\sqrt{7}}{704\pi^2}\beta_3\beta_4$ $=1.08\beta_3$ $+0.40\beta_2\beta_3+0.79\beta_3\beta_4$	$\frac{35}{16\sqrt{7\pi}}\beta_4+\frac{45}{16\pi}\beta_2^2$ $+\frac{215\sqrt{5}}{352\pi}\beta_2\beta_4+\frac{315}{176\pi}\beta_3^2+\frac{43305}{36608\pi}\beta_4^2$ $=1.23\beta_4+0.90\beta_2^2$ $+0.43\beta_2\beta_4+0.57\beta_3^2+0.38\beta_4^2$
$1 + \sum_{m=2}^4 \beta_m Y_{m,m}$ ε_n (tip-tip)	$\frac{320}{\sqrt{378}\pi^2}\beta_2\beta_3+\frac{800}{33\pi^2\sqrt{2}}\beta_3\beta_4$ $=1.67\beta_2\beta_3+1.74\beta_3\beta_4$	$\sqrt{\frac{15}{4\pi}}\beta_2+\frac{15}{\sqrt{21}\pi}\beta_2\beta_4-\frac{15}{8\pi}\beta_2^2$ $=1.09\beta_2+1.0\beta_2\beta_4-0.6\beta_2^2$	$\frac{64}{\pi\sqrt{70\pi}}\beta_3$ $-\frac{12\sqrt{6}}{\sqrt{7}\pi^2}\beta_2\beta_3-\frac{81}{16\sqrt{2}\pi^2}\beta_3\beta_4$ $=1.37\beta_3$ $-1.13\beta_2\beta_3-0.36\beta_3\beta_4$	$\sqrt{\frac{35}{4\pi}}\beta_4+\frac{15}{4\pi}\beta_2^2$ $-\frac{\sqrt{525}}{4\pi}\beta_2\beta_4-\frac{105}{32\pi}\beta_4^2$ $=1.67\beta_4+1.19\beta_2^2$ $-1.82\beta_2\beta_4-1.04\beta_4^2$
$\langle\varepsilon_n^2\rangle$ (same rotation)	$\frac{4096}{3675\pi^3}\beta_3^2=0.036\beta_3^2$	$\frac{3}{2\pi}\beta_2^2=0.477\beta_2^2$	$\frac{4096}{245\pi^3}\beta_3^2=0.539\beta_3^2$	$\frac{35}{18\pi}\beta_4^2+\frac{45}{14\pi^2}\beta_2^4$ $=0.62\beta_4^2+0.32\beta_2^4$
$\langle\varepsilon_n^2\rangle$ (indep. rotation)	$\frac{2048}{3675\pi^3}\beta_3^2=0.018\beta_3^2$	$\frac{3}{4\pi}\beta_2^2=0.239\beta_2^2$	$\frac{2048}{245\pi^3}\beta_3^2=0.270\beta_3^2$	$\frac{35}{36\pi}\beta_4^2+\frac{45}{28\pi^2}\beta_2^4$ $=0.31\beta_4^2+0.16\beta_2^4$

assumed to have a hard core of 0.4 fm in radii, with a density described by Eq. (1). The nuclear radius R_0 and the surface thickness a_0 are chosen to be $R_0 = 6.81$ fm and $a_0 = 0.55$ fm for ^{238}U and $R_0 = 5.09$ fm and $a_0 = 0.52$ fm for ^{96}Zr, respectively. The nucleon-nucleon inelastic cross sections are chosen to be $\sigma_{\mathrm{nn}} = 42$ mb at $\sqrt{s_{NN}} = 200$ GeV. In each collision event, nucleons are generated in each nuclei at a random impact parameter from each other. Each nucleus is then rotated by randomly generated three Euler angles before they are set on a straight line trajectory towards each other along the z direction. From this, the nucleons in the overlap region, known as participants, are identified. The ε_n are calculated from nucleon participants according to Eq. (2), and the results are studied as a function of N_{part}. For a systematic study of the influence of different shapes, one deformation component or particular combination of components of the same n is enabled at a time, the latter is useful to understand the influence of departure from axial and/or reflection symmetry. A special study is performed to also investigate the presence of shapes of different n, where two or three nonzero values for β_2, β_3, and β_4 are enabled simultaneously.

It is well known that the particle production in nucleus-nucleus collisions only scales approximately with N_{part}. A better scaling can be achieved by considering the constituent quarks as an effective degree of freedom for particle production [39–43], which would naturally give rise to different ε_n in each event. Defining centrality with constituent quarks is also expected to change the fluctuations of eccentricity [44], and provide a way to quantify the centrality smearing effects.

For this purpose, a quark Glauber model from Ref. [41] is used. Three quark constituents are generated for each nucleon according to the "mod" configuration [45], which ensures that the radial distribution of the three constituents after recentering follow the proton form factor $\rho_{\mathrm{proton}}(r) = e^{-r/r_0}$ with $r_0 = 0.234$ fm [46]. The value of quark-quark cross section is chosen to be $\sigma_{\mathrm{qq}} = 8.2$ mb in order to match the σ_{nn}. The ε_n are then calculated from the list of quark participants in the overlap region, and the number of quark participants N_{quark} is used as an alternative centrality estimator. In the quark Glauber model, I also explicitly keep track of the participant nucleons, i.e., a nucleon is counted as participant as long as one of its quarks participate in the collision. This paper presents and compares results obtained from both nucleon participants and quark participants.

In the presence of large deformation, the total volume of the nucleus increases slightly for fixed R_0 [47]. Considering the quadrupole deformation only, for the largest value considered, $\beta_2 = 0.34$, the ratio to the original volume is approximately $1 + \frac{3}{4\pi}\beta_2^2 + \frac{\sqrt{5}}{28\pi^{3/2}}\cos(3\gamma)\beta_2^3 = 1.021 + 0.0004\cos(3\gamma)$. In order to keep the overall volume fixed, it would require a small, less than 1%, decrease of R_0, which is safely ignored in the present study.

III. RESULTS

The goal of this paper is to explore the relation between $\langle\varepsilon_n^2\rangle$ and various deformation parameters in Eq. (1), and to provide insights on the deformation dependence of
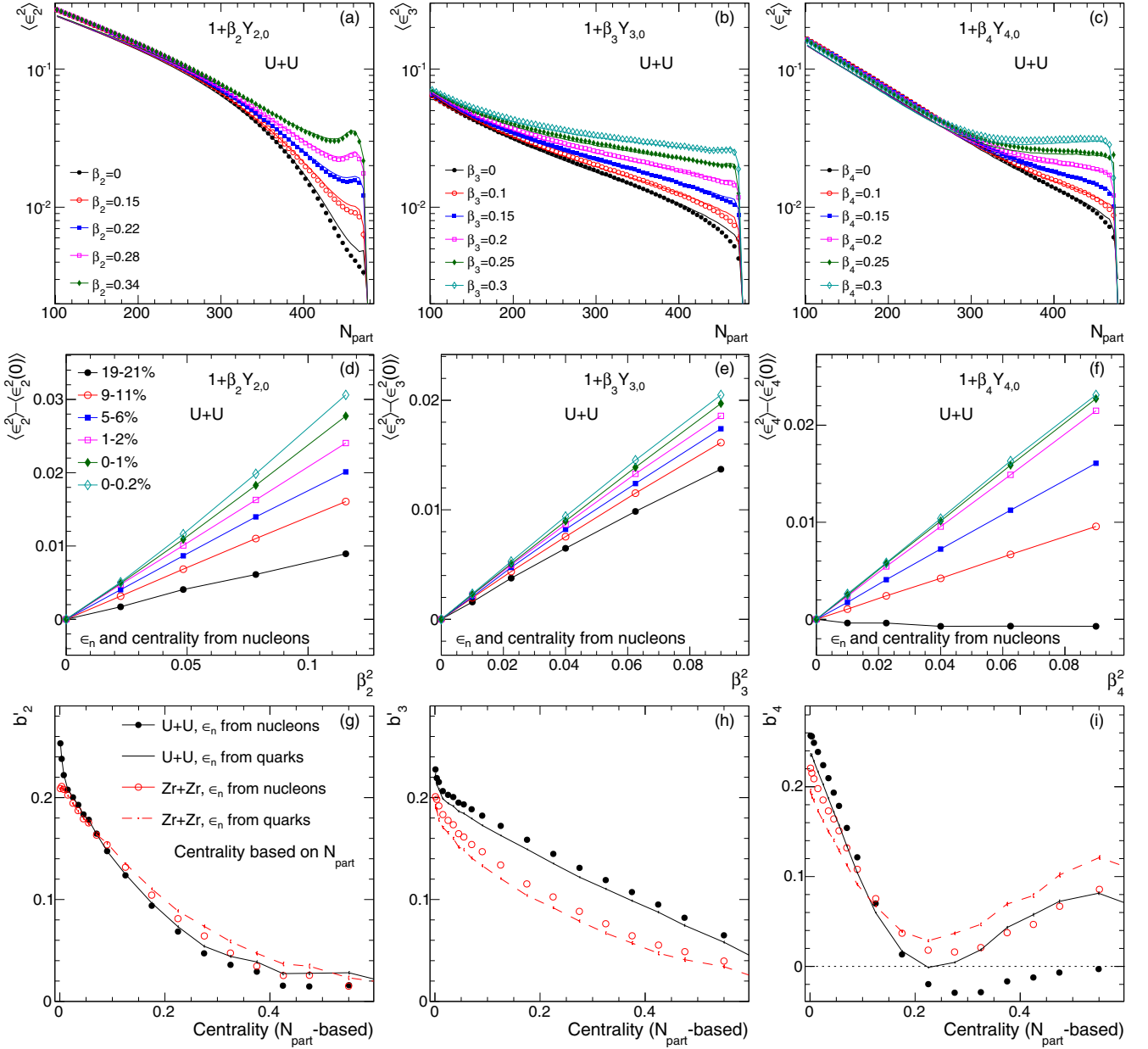
FIG. 2. Top row: The N_{part} dependence of mean square eccentricity $\langle \varepsilon_n^2 \rangle$ for several β_n values considering only the $Y_{n,0}$ component, with markers and lines corresponding to $d_\perp$ obtained with nucleons and quarks, respectively. Middle row: The β_n^2 dependence of $\langle \varepsilon_n^2 \rangle$ in several centrality ranges based on N_{part}, which can be nicely described by a linear function $\langle \varepsilon_n^2 \rangle - \langle \varepsilon_n^2 \rangle_{\beta_n=0} = b'_n \beta_n^2$. Bottom row: the centrality dependence of the slope parameter b'_n in U + U (black) and Zr + Zr (red) systems for ε_n calculated based on nucleons (markers) or quarks (lines). The results are shown for $n = 2$ (left column), $n = 3$ (middle column), and $n = 4$ (right column). The first three points in the bottom panels correspond to 0–0.2%, 0.2–0.5%, and 0.5–1%, respectively.

experimentally measured $\langle v_n^2 \rangle$. The influence of nuclear deformation on higher-order cumulants of ε_n will be explored in a separate study. Section III A establishes the quadratic relation (3) by considering the axial-symmetric deformation $Y_{n,0}$, $n = 2, 3$, and 4. The influences of nonaxial deformation, $Y_{n,m\neq 0}$, characterized by the triaxiality parameter γ and $\alpha_{n,m}$ parameters are considered in Sec. III B. One finds that the slope parameters $b'_{n,m}$ have a very weak dependence on the γ and $\alpha_{n,m}$. Section III C considers the presence of multiple shape components β_2, β_3, and β_4, which is generally ex-

pected in nuclear structure physics. For moderate deformation values, one finds that the nonlinear contributions, terms like $\beta_n \beta_m$, $m \neq n$, are subdominant and Eq. (3) still holds well. Section III D discusses ways to constrain these deformations simultaneously using flow measurements.

A. Influence of axial-symmetric multipole deformation

The top row of Fig. 2 shows the N_{part} dependence of $\langle \varepsilon_n^2 \rangle$, $n = 2, 3$, and 4, for various β_n values in U + U collisions, calculated from the participating nucleons according to Eq. (2).

One observes that the larger β_2 values increase ε_2 mostly in the central region, while larger β_3 values increase ε_3 over the full centrality range. The reason is that the contribution associated with the average elliptic geometry to ε_2 dominates over the deformation effects in the mid-central and peripheral collisions. On the other hand, the ε_3 without nuclear deformation arises solely from random fluctuations of nucleon positions and has a much smaller value, therefore the ε_3 is more sensitive to β_3. The increase of ε_4 with β_4 is observed only in the central region. In fact, the peripheral region shows a slight decrease of ε_4 with β_4. Overall, the influence of deformation on ε_n is largest in the most central region for all harmonics.

In the same plots, I also show the $\langle \varepsilon_n^2 \rangle$ calculated from quark participants as solid lines, with the same color as those calculated from nucleon participants. Small differences are observed in the UCC region when β_n are small, or in the peripheral region for $n = 2$, implying that the influences of deformation are insensitive to nucleon substructures.

To quantify these dependencies, $\langle \varepsilon_n^2 \rangle$ values obtained for fixed N_{part} are averaged in narrow centrality ranges, and plotted as a function of β_n^2 in the middle row of Fig. 2. A linear dependence is observed in all cases, confirming the first part of the relation in Eq. (3) involving a_n' and b_n'. Note that a_n' correspond to eccentricities in the absence of deformation, $a_n' = \langle \varepsilon_n^2 \rangle|_{\beta_n=0}$, shown by the black solid circles in the top row, while b_n' describes the slope of the β_n^2 dependencies in the middle row.

The bottom row of Fig. 2 shows the centrality dependence of b_n' for U + U and Zr + Zr collisions. The values of b_n' are largest in the UCC region and decrease toward mid-central and peripheral regions. It is quite remarkable that the value of b_n' starts at around 0.2–0.3 for all harmonics in both collision systems. This value of b_n' reflects an effect that is purely geometrical. If the two nuclei were to collide head-on in the direction perpendicular to maximum deformation as shown in Fig. 1, b_n' should be on the order of unity; see Table I. In reality, after averaging over all possible random orientations, the b_n' values are reduced to about 0.2–0.3. In a Monte Carlo Glauber model with finite number of nucleons, the random fluctuation of nucleon positions smear the correlation between the shape of the overlap region and the N_{part}. This smearing is expected to be larger for smaller system, leading to a slightly smaller b_n' in the Zr + Zr collisions than in the U + U collisions. Note that the centrality and collision system dependencies of b_n' are just the opposite of a_n' (the latter corresponds to the $\langle \varepsilon_n^2 \rangle$ without deformation shown in the top row). The values for a_n' are smallest in the UCC region and increase towards more peripheral regions and exhibit a much larger difference between Zr + Zr and U + U.

The bottom row of Fig. 2 also compares the b_n' calculated from nucleon participants with that calculated from quark participants. In the central and mid-central collisions, the differences are negligible for $n = 2$, but for $n = 3$ and $n = 4$ the results based on quark participants are systematically smaller. At this point, one may wonder if the ε_n are also affected by the β_m of different order, $m \neq n$. I have performed such calculations. In most cases, the influences are small. But I identified three cases for which the influences are quite large.

In particular, I find that the octupole deformation contributes strongly to the dipolar eccentricity in all centralities, and the hexadecapole deformation contributes to both dipolar and triangular eccentricities in the mid-central collisions. They are presented in Fig. 3 with a layout similar to Fig. 2. As these contributions are a global geometry effect with a radial distribution different from contributions arising from random fluctuation in nucleon positions in each event, they probably will be damped differently by viscous effects in comparison to a_n'. Similar effects are known in the context of hydrodynamic model studies as leading and subleading eccentricities, which characterize different length scales in the radial direction for ε_n, and subleading ε_n with higher frequency in radial direction is more damped than the leading ε_n [48,49]. Results for other $b_{n,m}'$ can be found in Figs. 10–13 in Appendix B, including the quartic dependence of $\langle \varepsilon_4^2 \rangle$ on β_2 predicted in Table I.

The middle row of Fig. 3 shows that contributions between different orders also follow a quadratic dependence, confirming the second part of Eq. (3). The slopes, $b_{1,3}'$, $b_{1,4}'$, and $b_{2,4}'$, are summarized in the bottom row of Fig. 3. One should not be tricked by the apparent small value of $b_{1,3}'$, though. Since the value of a_1', the $\langle \varepsilon_1^2 \rangle$ without deformation, is very small in the UCC region, even a value of $b_{1,3}' = 0.015$ together with a modest octupole deformation of $\beta_3 = 0.1$ could increase the $\langle \varepsilon_1^2 \rangle$ by about 15%. In mid-central collisions, due to a much larger a_1', the combined contributions from $\beta_3 = 0.1$ and $\beta_4 = 0.1$ are less than 10%. This result suggests that the dipolar flow in the UCC region could in principle be used to probe the octupole deformation. On the other hand, the influence of β_4 on ε_3 is significant in the mid-central collisions, and is negligible in the UCC region. The bottom row of Fig. 3 also compares the slope parameters between U + U and Zr + Zr collisions; they are very similar in the UCC region, but values in Zr + Zr are about 20% smaller in the mid-central collisions.

To summarize the main message of Fig. 3, the ε_n for $n = 2$, 3, and 4 in the UCC region are not affected by deformations of different order β_m, $m \neq n$, leading to a particularly simple expression, $\langle \epsilon_n^2 \rangle_{\mathrm{UCC}} = a_n' + b_n' \beta_n^2$. Exploiting this relation in the UCC collisions from experimentally measured v_n values provides a clean way to constrain the β_n parameters, as will be discussed in Sec. III D.

B. Influence of nonaxial deformations

I first consider the influence of triaxiality parameter γ, which mixes the contribution from Y_{20} and Y_{22} components, while keeping the overall magnitude of quadrupole deformation β_2 fixed. The top-left panel of Fig. 4 shows the N_{part} dependence of $\langle \varepsilon_2^2 \rangle$ for $\beta_2 = 0.28$ but different γ values in the U + U collisions. They are contrasted to the case for spherical nuclei $\beta_2 = 0$. It is clear that, over most of the centrality range, $\langle \varepsilon_2^2 \rangle$ have very little sensitivity to γ. The $\langle \varepsilon_2^2 \rangle$ calculated with quark participants, shown as solid lines in the same panel, also give very similar results.

To test the influence of volume/centrality fluctuations, results obtained using N_{quark} as centrality are shown in the top-right panel. Large splittings between different γ cases are observed in the UCC region of 0–1%. Namely, the $\langle \varepsilon_2^2 \rangle$ for oblate deformation $\gamma = \pi/3$ shows a stronger increase as a
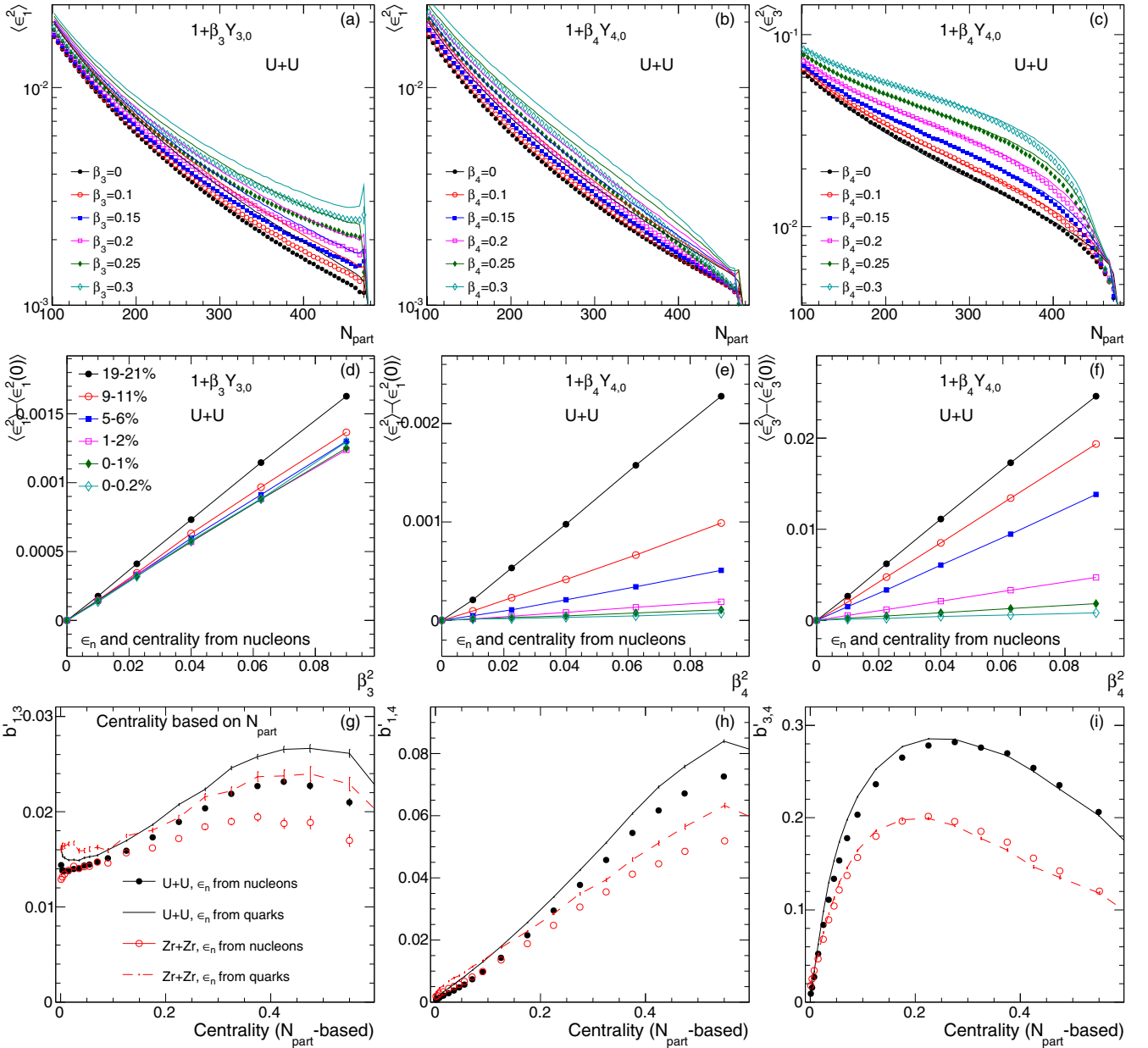
FIG. 3. Characterization of the influence of β_3 to $\langle \varepsilon_1^2 \rangle$ (left column), β_4 to $\langle \varepsilon_1^2 \rangle$ (middle column), and β_4 to $\langle \varepsilon_3^2 \rangle$ (right column). The top row shows the centrality dependence of $\langle \varepsilon_n^2 \rangle$ for several values of β_3 or β_4 as indicated in the panels, with markers and lines corresponding to $d_\perp$ obtained with nucleons and quarks, respectively. The middle row shows the β_3^2 or β_4^2 dependence of $\langle \varepsilon_1^2 \rangle$ or $\langle \varepsilon_1^2 \rangle$ in several centrality ranges. The bottom row shows the centrality dependence of the extracted slope parameter $b'_{1,3}$ (left), $b'_{1,4}$ (middle), or $b'_{3,4}$ (right) for U + U (black) and Zr + Zr (red) systems for ε_n calculated based on nucleons (markers) or quarks (lines). The first three points in the bottom panels correspond to 0–0.2%, 0.2–0.5%, and 0.5–1%, respectively.

function of N_{quark} before they all start to decrease slightly at the largest N_{quark} values. This behavior suggests that the events selection based on N_{part} or N_{quark} have different correlation with, and therefore different sensitivity to, the triaxiality of the nucleus. The largest difference is reached between the prolate deformation and the oblate deformation, consistent with a previous study based on the AMPT model [11,36]. In that study, a similar dependence on γ is observed for the final-state v_2. Interestingly, the U + U v_2 data from the STAR Collaboration show a decreasing behavior as a function of N_{ch} in the UCC

region, while the Au + Au v_2 data show a slight rising trend [29], compatible with a prolate deformation of ^{238}U nucleus and a oblate deformation of ^{197}Au. In summary, my results suggest that the two-particle correlators $\langle v_2^2 \rangle$ are sensitive to the triaxiality only in the UCC region, and the level of sensitivity depends on the choice of centrality estimator.

The middle row of Fig. 4 quantifies the γ dependence of $\langle \varepsilon_2^2 \rangle$ in several centrality ranges in N_{part} on the left and N_{quark} on the right in the U + U collisions. The γ dependence is well described by a linear function of $\cos(3\gamma)$, reflecting the
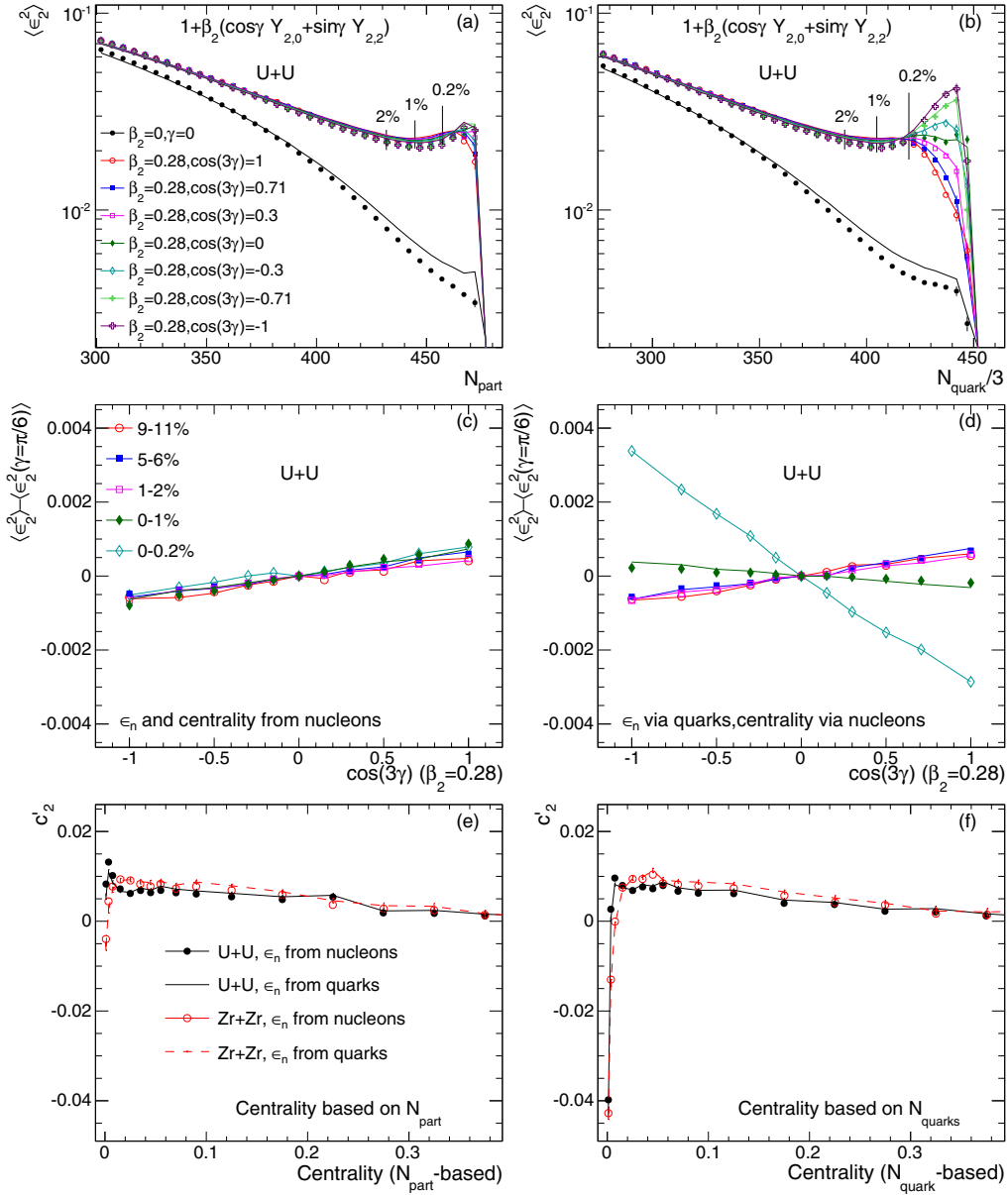
FIG. 4. Characterization of the influence of triaxiality γ on $\langle \varepsilon_2^2 \rangle$. Top row: The $N_{\rm part}$ (left) and $N_{\rm quark}$ (right) dependencies of $\langle \varepsilon_2^2 \rangle$ for different values of γ, where markers and lines correspond $d_\perp$ obtained with nucleons and quarks, respectively. Middle row: $\langle \varepsilon_2^2 \rangle - \langle \varepsilon_2^2(\gamma = \pi/6) \rangle$ as a function of $\cos(3\gamma)$ in several centrality ranges based on $N_{\rm part}$ (left) and $N_{\rm quark}$ (right), which follows a linear function of $\cos(3\gamma)$, whose slope is parametrized as $c_2' \beta_2^2$ [see Eq. (4)]. Bottom row: the extracted c_2' as a function of centrality for U + U (black) and Zr + Zr (red) systems for ε_n calculated based on nucleons (markers) or quarks (lines). The first three points in the bottom panels correspond to 0–0.2%, 0.2–0.5%, and 0.5–1%, respectively.

expected threefold periodicity. A similar observation is also made in the Zr + Zr collisions, although the sensitivity to γ is observed over a larger centrality range. Based on this finding, I arrive the following empirical formula that accounts for the dependence on both β_2 and γ:

$$\langle \varepsilon_2^2 \rangle = a_2' + [b_2' + c_2' \cos(3\gamma)]\beta_2^2. \tag{4}$$

Note that the $c_2'\beta_2^2$ is the slope of the $\cos(3\gamma)$ dependence in the middle row of Fig. 4. The bottom row of Fig. 4 shows the centrality dependence of c_2'. The value of c_2' is generally much smaller than b_2', $c_2' \ll b_2'$, and approaches zero in the periph-

eral collisions. However, its value in the UCC region changes sign and could gain a sizable magnitude depending on the centrality estimator. Lastly, for other eccentricities $\varepsilon_n, n \neq 2$, only very small dependencies on the triaxiality are observed, typically less than 5%. However, these dependencies to a good extent can also be described by a $\cos(3\gamma)$ function (see the left column of Figs. 10–13).

This result prompts the question of whether the finding about triaxiality also applies for the octupole and hexade-capole deformations. These higher-order deformations have many more shape parameters. In the intrinsic frame defined
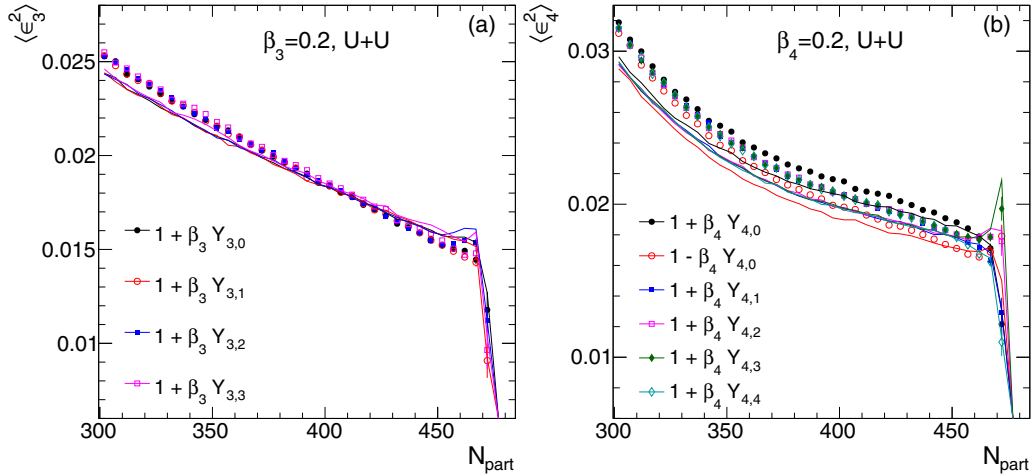
FIG. 5. Left: The N_{part} dependence of $\langle \varepsilon_3^2 \rangle$ for different components of octupole deformation $Y_{3,m}$ with a deformation value of $\beta_3 = 0.2$. Right: The N_{part} dependence of $\langle \varepsilon_4^2 \rangle$ for different components of octupole deformation $Y_{4,m}$ with a deformation value of $\beta_4 = 0.2$. The ε_n are calculated either from nucleons (symbols) or quarks (lines). For all cases $\beta_2 = 0$.

by the quadrupole deformation, after taking out the β_n that describe the overall strength of the deformation, there are still six and eight independent shape variables for octupole and hexadecapole deformations, respectively. Besides, there are also large redundancies in the parameter space due to spatial symmetry of spherical harmonics. For example, if the underlying quadrupole deformation is axial symmetric, terms like $\cos(\delta) Y_{n,m} + \sin(\delta) Y_{n,-m}$ can be absorbed by an azimuthal rotation of $Y_{n,m}$ without real physical consequence. There have been several attempts to find efficient parametrizations to reduce this redundancy; see Refs. [50,51]. My paper follows a more relaxed approach, where I just test special cases of the octupole and hexadecapole shapes. It is reassuring that $\langle \varepsilon_n^2 \rangle$ has very small sensitivity to these internal angular parameters, as will be described below.

For this study, I consider all real valued spherical harmonics $Y_{3,m}$ and $Y_{4,m}$. They are introduced one at a time in the Glauber model and the resulting ε_n are calculated. The results are summarized in Fig. 5. I found that ε_3 values are the same for all $Y_{3,m}$ components, except for small differences in the UCC region. I also tried several combinations, such as $\cos(\delta) Y_{3,0} + \sin(\delta) Y_{3,1}$ with δ a free mixing angle, and the conclusion remains the same. I suspect that this is true for general mixing of all components $\alpha_{3,m}$ in Eq. (1), as long as $\sum_{m=-3}^{3} \alpha_{3m}^2 = 1$ is satisfied. This independence is also observed for β_3 contribution to the dipolar eccentricity ε_1 and probably is a property for all odd-order deformations.

On the other hand, the $\langle \varepsilon_4^2 \rangle$ values show modest differencexs, at a level of 15%, among different $Y_{4,m}$ components for $\beta_4 = 0.2$. Results for nonaxial components $1 + \beta_4 Y_{4,m}, m \neq 0$ lie exactly between $1 + \beta_4 Y_{4,0}$ and $1 - \beta_4 Y_{4,0}$. The differences are largest in central collisions but are present throughout the entire centrality range. This is different from $\langle \varepsilon_2^2 \rangle$, for which the dependence on the triaxiality is observed only in the UCC region. I initially thought that the $\langle \varepsilon_4^2 \rangle$ for the most general hexadecapole shape should be in between the results for Y_{40} and $-Y_{40}$, which turns out is not the case. In fact, the extrema of $\langle \varepsilon_4^2 \rangle$ are reached for deformation described by $\sqrt{7/12} Y_{4,0} +$

$\sqrt{5/12} Y_{4,4}$ and $\sqrt{5/12} Y_{4,0} - \sqrt{7/12} Y_{4,4}$, with the maximum for $\beta_4 = |\beta_4|$ and minimum for $\beta_4 = -|\beta_4|$ [51]. Identifying heavy ion observables that are sensitive to the sign of β_4 will be particularly useful for understanding nuclear fission data [52]. A more detailed investigation of this topic is given in Appendix B.

C. Simultaneous presence of quadrupole-octupole-hexadecapole deformations

Although the axial quadrupole distortion is the nuclear deformation of primary importance, secondary contributions from octupole and hexadecapole components often coexist and can be important in some regions of nuclear chart [53]. One example is the pear-shaped ^{224}Ra [54] with a $(\beta_2, \beta_3, \beta_4)$ value of (0.1545, 0.097, 0.080) [55]. A summary of the deformation parameters for the large systems collided at RHIC and the LHC is given in Table II, highlighting the importance of possible higher-order deformations. It would be interesting to study how the eccentricities depend on the simultaneous presence of these different deformations; in particular, whether the contribution from each component to ε_n is independent of each other.

For this exploratory study, only combinations of axial-symmetric components $Y_{n,0}, n = 2, 3, 4$ are considered, from

TABLE II. Some estimates of the deformation values β_2, β_3, and β_4 for tlarge nuclei collided at RHIC and the LHC with references given, mostly based on global analysis of the $B(En)$ transition data.

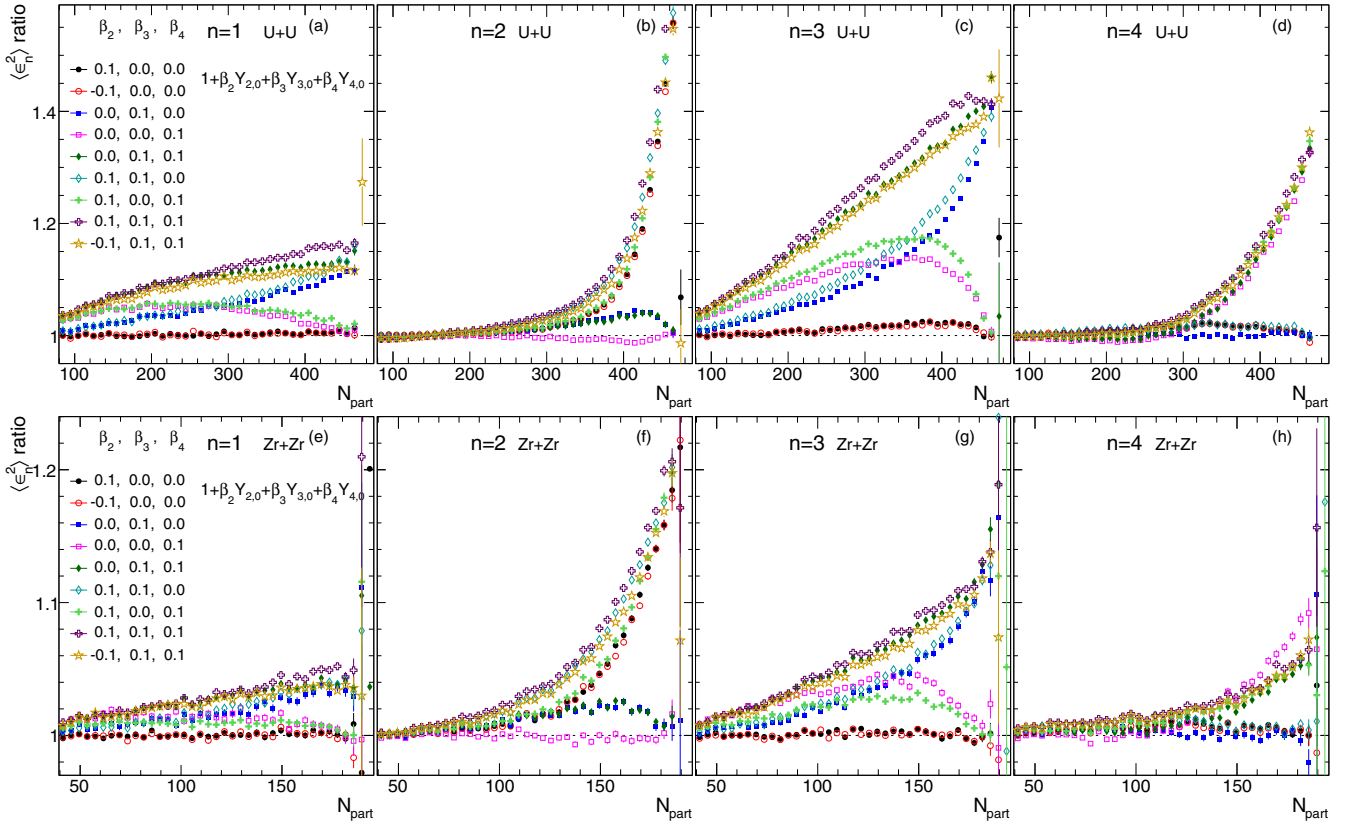|	β_2	β_3	β_4
^{238}U	0.286 [56]	0.078 [57]	0.07–0.09 [58,59]
^{208}Pb	0.05 [56]	0.04 [60]	
^{197}Au	$-(0.13–0.16)$ [59,61]		-0.03 [59]
^{129}Xe	0.16 [59]		
^{96}Ru	0.05–0.16 [56,59]		
^{96}Zr	0.08 [56]	0.20–0.27 [62]	0.06 [59]

FIG. 6. Relative change of $\langle \varepsilon_1^2 \rangle$ (left column), $\langle \varepsilon_2^2 \rangle$ (second column), $\langle \varepsilon_3^2 \rangle$ (third column), $\langle \varepsilon_4^2 \rangle$ (rightmost column) for U + U (top row) and Zr + Zr (bottom row) collisions, relative to the undeformed case, for different combinations of β_2, β_3, and β_4 as indicated in the left panels. Only the axial components of the deformation, $Y_{2,0}$, $Y_{3,0}$, and $Y_{4,0}$, are considered.

which the ε_1, ε_2, ε_3, and ε_4 are calculated. The analysis is carried out for different combinations of $(\beta_2, \beta_3, \beta_4)$ from the values $\beta_2 = \pm 0.1, 0$, $\beta_3 = 0.1, 0$, and $\beta_4 = 0.1, 0$. The results for U + U and Zr + Zr, in terms of ratios to the spherical nuclei, are shown in Fig. 6. The contributions to eccentricities from different deformation components are almost independent of each other, i.e., following Eq. (3). Modest deviations are observed in a few cases, however. In particular, the ε_2 is observed to increase with β_3 in noncentral region, and the difference of ε_n between $\beta_2 = 0.1$ and -0.1 is also larger when β_3 and/or β_4 are nonzero. Remarkably, such nonlinear effects are very small in the UCC region, where ε_n is only sensitive to β_n except for $n = 1$. For the odd harmonics ε_1 and ε_3, both β_3 and β_4 can have large contribution in noncentral collisions.

Figure 7 considers a different scenario where the quadrupole component is much larger than the octupole and hexadecapole. For this case, I increase the β_2 to the value of 0.28. Most trends remain qualitatively the same as Fig. 6. In particular, the ε_1 and ε_3 over most the centrality range, as well as ε_4 in the UCC region, are still dominated by the β_3 and β_4. The behaviors for $(\beta_2, \beta_3, \beta_4) = (0.28, 0.1, 0.1)$ for ^{238}U, comparable to the values obtained from nuclear structure calculations in Table II, are particularly interesting. A significant enhancement of $\langle \varepsilon_3^2 \rangle$ of about 40% is expected in the central collisions relative to the case of no deformation. Since $\langle \varepsilon_3^2 \rangle \propto 1/A$ without deformation in a large system, the

$\langle \varepsilon_3^2 \rangle$ in the UCC Au + Au collisions should be $238/197 - 1 = 21\%$ larger than those in the UCC U + U collisions. Therefore in the presence of nonzero β_3 and β_4, the ordering is expected to be flipped: the $\langle \varepsilon_3^2 \rangle_U$ is expected to be 20% larger than $\langle \varepsilon_3^2 \rangle_{Au}$, and consequently $\langle v_3^2 \rangle_U$ is expected to be larger than $\langle v_3^2 \rangle_{Au}$. The reverse ordering of v_3 between U + U and Au + Au collisions, if observed, would be a strong indication for the presence of octupole deformation in ^{238}U nucleus.

Another useful example is the ^{96}Zr + ^{96}Zr and ^{96}Ru + ^{96}Ru isobar collisions taken by the STAR Collaboration in 2018. The ratio $\langle v_n^2 \rangle_{Zr}/\langle v_n^2 \rangle_{Ru}$ will directly constrain the relative ordering of $\beta_{n,Zr}$ and $\beta_{n,Ru}$ [63], especially in the UCC region, where other effects associated with the radial distribution of nucleons, such as neutron skin, are less important [64,65]. Therefore observation of significant deviation of the ratio $\langle v_3^2 \rangle_{Zr}/\langle v_3^2 \rangle_{Ru}$ from unity with the characteristic centrality dependence, similar to that shown in the bottom panels of Fig. 6, would be strong evidence for the presence of octupole correlations in these isobar systems.

In summary, the contributions of deformation to ε_n arise mainly from β_n for $n = 2$, 3, and 4. In particular, there are small cross-contributions and nonlinear effects between β_2 and ε_3 and between β_3 and ε_2, especially in the UCC region. This should be contrasted to the well-known anticorrelation between $a_2' = \langle \varepsilon_2^2 \rangle_{|\beta_n = 0}$ and $a_3' = \langle \varepsilon_3^2 \rangle_{|\beta_n = 0}$ in the absence of
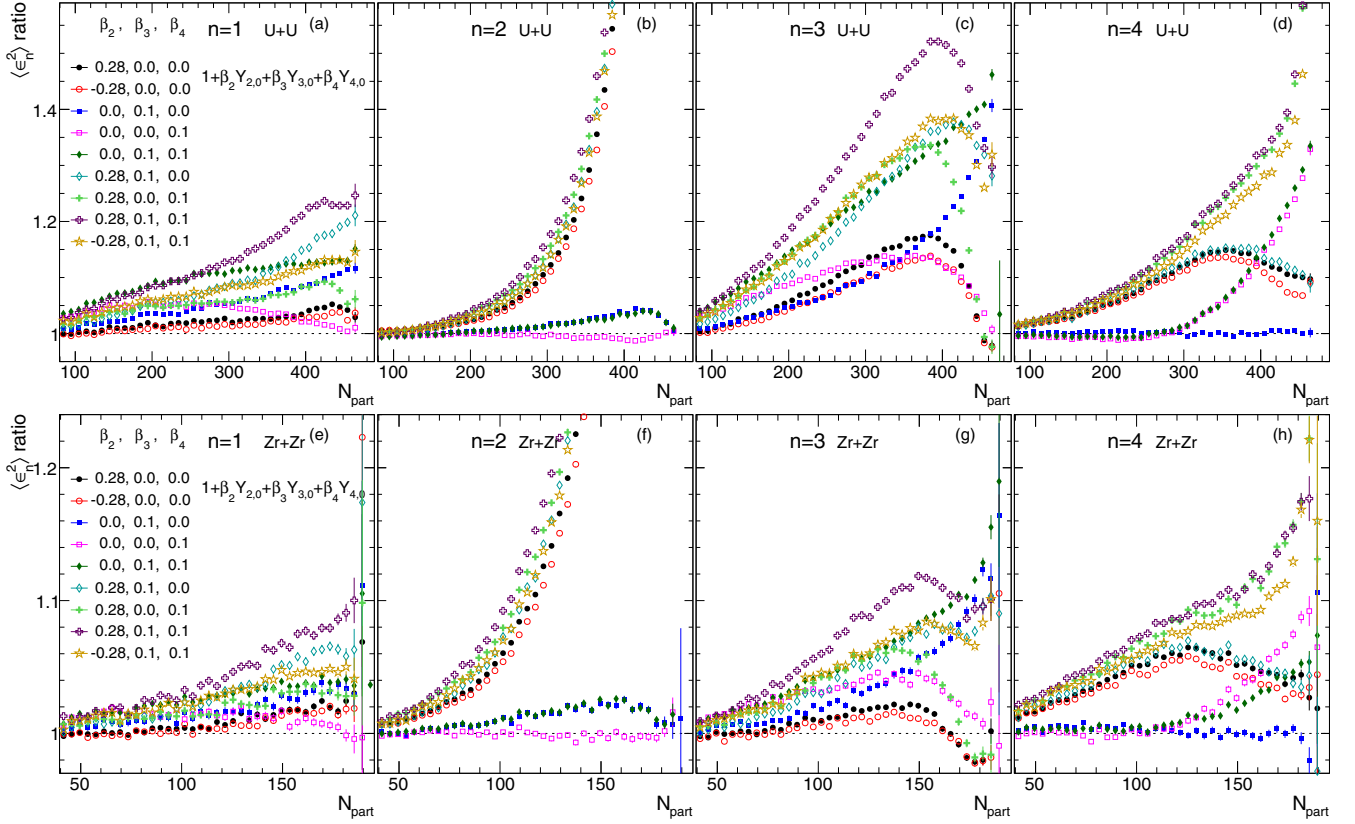
FIG. 7. Relative change of $\langle \varepsilon_1^2 \rangle$ (left column), $\langle \varepsilon_2^2 \rangle$ (second column), $\langle \varepsilon_3^2 \rangle$ (third column), $\langle \varepsilon_4^2 \rangle$ (rightmost column) for U + U (top row) and Zr + Zr (bottom row) collisions, relative to the undeformed case, for different combinations of β_2, β_3, and β_4 as indicated in the left panels. Only the axial components of the deformation, $Y_{2,0}$, $Y_{3,0}$, and $Y_{4,0}$ are considered. The only difference from Fig. 6 is that a larger β_2 value of 0.28 is considered.

nuclear deformation [66], where ε_3 arises from random position fluctuations of nucleons, the latter having opposite effects for ε_3 and ε_2. Therefore, one can constrain the values of β_2, β_3, and β_4 by combining the information from v_1, v_2, v_3, and v_4 in the ultracentral collisions, as will be discussed next.

D. Constraining quadrupole, octupole, and hexadecapole deformations using collective flow data

Exploiting the linear dependence of between ε_2^2 and β_2^2, I previously proposed a method [11] to relate the quadrupole deformation between two collision systems of similar sizes. This method can be straightforwardly generalized to octupole and hexadecapole deformations.

Recall that, in the UCC region, v_n for $n = 2$–4 depends linearly on ε_n, and ε_n is sensitive only to β_n according to Eq. (3). Therefore, one expects that the v_n in the UCC region to also follow a similar dependence on β_n,

$$\langle v_n^2 \rangle = a_n + b_n \beta_n^2, \quad n = 2, 3, 4, \tag{5}$$

where averages are performed over events in a narrow centrality class and $a_n = \langle v_n^2 \rangle_{|\beta_n=0}$. Following the argument of Ref. [11], I write down a simple equation relating the deformation and flow in two collision systems $X + X$ and $Y + Y$ that are close in mass number, with subscript X (Y) indicating

a quantity evaluated in $X + X$ ($Y + Y$) collisions:

$$\beta_{n,Y}^2 = \left(\frac{r_{v_n^2} r_{a,n} - 1}{r_{n,Y}} \right) + \left(r_{v_n^2} r_{b,n} \right) \beta_{n,X}^2, \quad r_{v_n^2} \equiv \frac{\langle v_n^2 \rangle_Y}{\langle v_n^2 \rangle_X},$$

$$r_{b,n} = \frac{b_{n,X}}{b_{n,Y}}, \; r_{a,n} = \frac{a_{n,X}}{a_{n,Y}}, \; r_{n,Y} = \frac{b_{n,Y}}{a_{n,Y}}. \tag{6}$$

As shown in the bottom panels of Fig. 2, b_n' has very weak dependence on system size, therefore one expects it is true also for b_n and therefore $r_{b,n} \approx 1$. In the absence of deformation, $\beta_{n,X} = \beta_{n,Y} = 0$, using the linear response relation $\langle v_n^2 \rangle = k_n^2 \langle \varepsilon_n^2 \rangle$, the relative difference of harmonic flow between $X + X$ and $Y + Y$ collisions, $\Delta \langle v_n^2 \rangle / \langle v_n^2 \rangle = (\langle v_n^2 \rangle_X - \langle v_n^2 \rangle_Y) / \langle v_n^2 \rangle_Y$, can be decomposed as

$$\frac{\Delta \langle v_n^2 \rangle_{|\beta_n=0}}{\langle v_n^2 \rangle_{|\beta_n=0}} = \frac{\Delta k_n^2}{k_n^2} + \frac{\Delta \langle \varepsilon_n^2 \rangle_{|\beta_n=0}}{\langle \varepsilon_n^2 \rangle_{|\beta_n=0}} \rightarrow \frac{\Delta a_n}{a_n} = \frac{\Delta k_n^2}{k_n^2} + \frac{\Delta a_n'}{a_n'}. \tag{7}$$

In the UCC region, the eccentricities are dominated by the random fluctuations of nucleon positions and to a good extent can be approximated by $\langle \varepsilon_n^2 \rangle \propto 1/A$ [67,68], and therefore $\Delta \langle \varepsilon_n^2 \rangle / \langle \varepsilon_n^2 \rangle \approx \Delta \frac{1}{A} / \frac{1}{A}$. The response coefficient k_n is damped with the respect to the ideal hydrodynamic value, $k_{n,\text{ih}}$. In the simplified acoustic scaling scenario of Ref. [15,69–71], one
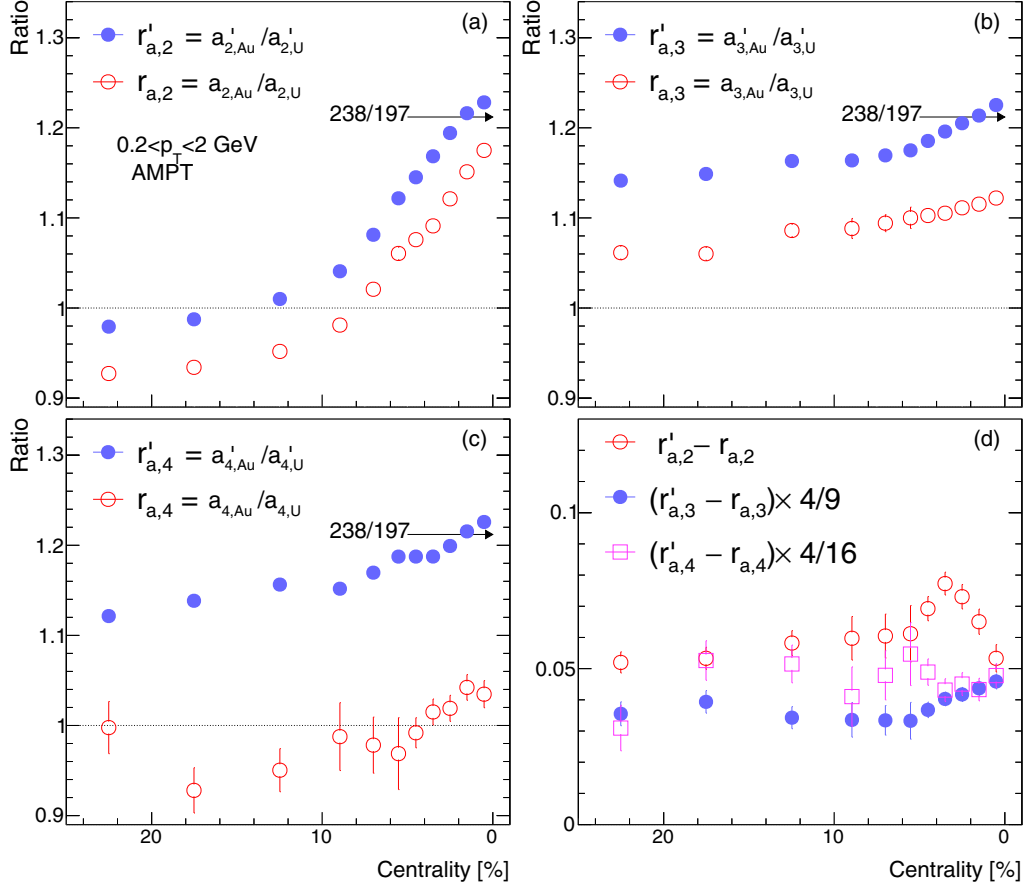
FIG. 8. The ratio of mean square eccentricity and mean square flow harmonics without deformation, $a'_n = \langle \varepsilon_n^2 \rangle_{\beta_n=0}$ and $a_n = \langle v_n^2 \rangle_{\beta_n=0}$, between Au + Au and U + U collisions for $n = 2$ (top left), $n = 3$ (top right), $n = 4$ (bottom left) as a function of centrality based on N_{ch} obtained from the AMPT model in Ref. [11]. The arrows indicate the expected ratios of ms eccentricity in the large system limit: $(1/A_{\text{Au}})/(1/A_{\text{U}}) = 238/197 = 1.21$. The bottom right panel shows the difference between $r'_{a,n} = a'_{n,\text{Au}}/a'_{n,\text{U}}$ and $r_{a,n} = a_{n,\text{Au}}/a_{n,\text{U}}$, scaled by the expected viscous damping factor according to Eq. (9).

has $k_n/k_{n,\text{ih}} \approx 1 - Kn^2$, where K encodes the viscous correction. This leads to $\Delta k_n/k_n \approx -\Delta K n^2 k_{n,\text{ih}}/k_n$. For central collisions of large systems [67], k_n is close to the ideal hydro limit, and $k_{n,\text{ih}}/k_n$ are nearly independent of n, therefore one obtains

$$\frac{\Delta k_n^2}{k_n^2} = \frac{n^2}{m^2}\frac{\Delta k_m^2}{k_m^2}. \qquad (8)$$

Combining Eqs. (7) and (8) yields two coupled equations,

$$r'_{a,2} - r_{a,2} = x_3(r'_{a,3} - r_{a,3}) = x_4(r'_{a,4} - r_{a,4}),$$

$$x_3 \approx \frac{4}{9}, \; x_4 \approx \frac{4}{16}. \qquad (9)$$

These equations involve only ratios of quantities between two systems close in size. All these ratios are close to unity and can be reliably estimated from the hydrodynamic model. I have verified these relations explicitly in the AMPT model simulation of Au + Au and U + U collisions without deformations in a previous study [11,36]. The centrality dependencies of these ratios are shown in Fig. 8 with $X = {}^{197}$Au, $Y = {}^{238}$U. It is immediately clear that $r_{a,n}$ follows closely the centrality dependence trends of $r'_{a,n}$, but has smaller

values due to viscous damping. The difference grows with n, reflecting the stronger viscous damping for higher-order flow harmonics. In the 0–1% most central collisions (the rightmost point for each dataset), one has $r'_{a,n} = 1.23$ independently of the harmonic number. This number is very close to the expected ratio of atomic numbers $(1/A_{\text{Au}})/(1/A_{\text{U}}) = 238/197 = 1.21$.

The bottom right panel demonstrates the robustness of Eq. (9). Using the viscous damping relation (8), the predicted values in the 0–1% most central collisions converge remarkably within 0.005 between different harmonics. But deviations from this scaling appear away from the most central region. For v_3, one finds a value of $x_3 = 5/9 \approx 0.55$ achieves best agreements over the 1%–25% centrality range as shown. This value is close to $x_3 = 0.57 \approx 5/9$ from a recent state-of-the-art hydrodynamic simulation [72]. For the v_4, I found $x_4 = 5/16 \approx 0.31$ has the best agreement in the 1%–25% centrality range, although the interpretation may be complicated by the mode-mixing contribution from elliptic flow that scales like $v_4 \sim v_2^2$, for which a smaller damping $x_4 = 8/16$ is expected [15]. For the remaining discussion, I shall focus simply on the 0–1% most central bin.

First, I use the approximation $\langle \varepsilon_n^2 \rangle_{|\beta_n=0} \propto 1/A$ and rewrite Eqs. (9) and (6) as

$$\beta_{n,Y}^2 = \frac{r_{v_n^2} r_{a,n} - 1}{r_{n,Y}} + r_{v_n^2} \beta_{n,X}^2, \quad r_{a,2} = (1 - x_3)\frac{A_Y}{A_X} + x_3 r_{a,3}$$

$$= (1 - x_4)\frac{A_Y}{A_X} + x_4 r_{a,4}, \quad x_3 \approx \frac{4}{9}, \ x_4 \approx \frac{4}{16}. \quad (10)$$

Presumably, if one deformation e.g., $n = 3$ is absent, $r_{a,3} = \langle v_{3,X}^2 \rangle_{|\beta_3=0} / \langle v_{3,Y}^2 \rangle_{|\beta_3=0}$ can be obtained directly from experiments, which allows me to fix $r_{a,2}$ and $r_{a,4}$ values. Alternatively, $r_{a,n}$ can be cross-calibrated by picking nuclei with similar mass number, therefore all of them are very close to unity. One such example is the Zr + Zr and Ru + Ru isobar datasets for which both $r_{b,n}$ and $r_{a,n}$ should be very close to unity.[3] The only variable that needs to be evaluated numerically in the hydrodynamic model is $r_{n,Y} = b_{n,Y}/a_{n,Y}$, which is the property of a single collision system.

One such numerical analysis has been performed in Ref. [11]; here I offer a bit more discussion on the expected behavior. Defining two response coefficients, $k_{b,n} = \sqrt{b_n/b_n'}$ and $k_{a,n} = \sqrt{a_n/a_n'}$, r_n can be rewritten as

$$r_n = \frac{b_n}{a_n} = \frac{k_{b,n}^2}{k_{a,n}^2} \frac{b_n'}{a_n'}. \quad (11)$$

The $k_{a,n}^2$ is the usual viscous damping coefficient for $\langle v_n^2 \rangle$ in the absence of deformation, while $k_{b,n}^2$ describes the damping of the β_n^2-dependent part of the $\langle v_n^2 \rangle$ in Eq. (5). From the AMPT model study, I found the ratio of the two damping coefficients for $n = 2$ is $k_{b,2}/k_{a,2} \approx 0.75$ in the UCC region in U + U collisions, and only has a very weak dependence on N_{part}, suggesting that $k_{b,2}/k_{a,2}$ is not very sensitive to viscosity. If this is the case, the model dependence lies in the ratio $r_n' = b_n'/a_n'$, whose uncertainty arises mainly from centrality smearing effects, e.g., the relative smearing of centrality based on the final state charged particle multiplicity N_{ch} and on N_{part}.

IV. DISCUSSION AND SUMMARY

The main finding of the paper is the simple parametric relation between ε_n and multipole deformation of nuclei β_n, $\langle \varepsilon_n^2 \rangle = a_n' + b_n' \beta_n^2$ for $n = 2$, 3, and 4, valid in all centralities and different collision systems. The a_n' reflects the eccentricities for spherical nuclei, i.e., $a_n' = \langle \varepsilon_n^2 \rangle_{|\beta_n=0}$. The a_2' is dominated by elliptic shape of the overlap region, which starts at a small value in central collisions and grows rapidly toward mid-central and peripheral collisions. Other a_n', $n \neq 2$ are generated by random fluctuations of participating nucleons and typically scales as $1/N_{part}$. On the other hand, β_n influences the global shape of the overlap region on an event-by-event bases, and its contribution to eccentricity $b_n' \beta_n^2$ plays a role similar to the so-called reaction plane ellipticity $\varepsilon_{2,RP}$ associated with the average elliptic shape of the
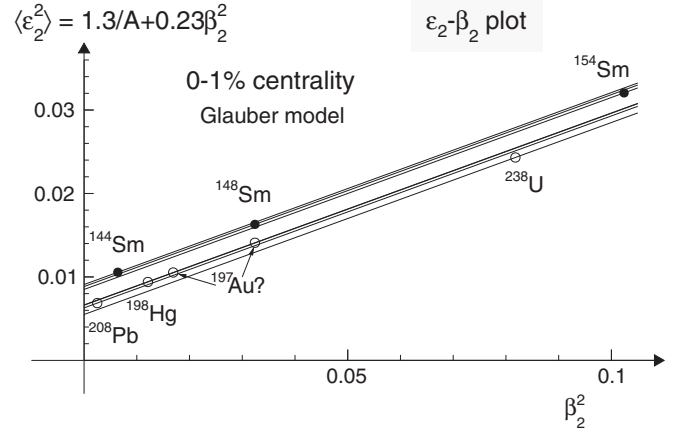
FIG. 9. Correlation of mean square elliptic eccentricity and β_2 in 0–1% centrality, $\langle \varepsilon_2^2 \rangle = a_2' + b_2' \beta_n$, estimated from the Glauber model for various large collision species, where is a_2' and b_2' are approximately $a_2' = 1.3/A$ and $b_2' = 0.23$. For even-even nuclei, the values of deformation come from low-energy data, as in Table II. For ^{197}Au, whose β_2 is not directly measured, I also include a recent estimate based on the v_2 data from Au + Au and U + U collisions, $|\beta_{2,Au}| \approx 0.18$ [11]. Offsets between different species are due to differences in mass numbers A, therefore each group of nuclei with very similar masses, (^{197}Au, ^{198}Hg, ^{208}Pb) or (^{144}Sm, ^{148}Sm, ^{154}Sm), almost fall on the same curve.

overlap. Due to linear response $v_n = k_n \varepsilon_n$ predicted by hydrodynamic models, I expect a similar dependence for v_n, $\langle v_n^2 \rangle = a_n + b_n \beta_n^2$. From these, I define deformation-dependent and deformation-independent hydrodynamic response coefficients $k_{b,n} = \sqrt{b_n/b_n'}$ and $k_{a,n} = \sqrt{a_n/a_n'}$. It would be insightful to investigate and compare $k_{a,n}$ and $k_{b,n}$, which will provide a new kind of test on the hydrodynamic models.

The best place to reveal nuclear deformation is the ultracentral collisions (UCC) of large systems, where the deformation-driven components become comparable to or even larger than the values without deformation. For this purpose, I propose a collision-system scan of a few species of similar size at RHIC to systematically establish the influence of deformation; see the sketch in Fig. 9.

First, it would be useful to scan two nuclei, e.g., ^{208}Pb and another species, in the vicinity of ^{197}Au, to improve the modeling of Au + Au collisions, providing information which is crucial for the precision interpretation of high-statistics flow data. Comparison between Pb + Pb at RHIC and the LHC will constrain any possible energy dependence of the initial state effects and pre-equilibrium dynamics. Since ^{208}Pb is nearly spherical, a comparison of Pb + Pb with Au + Au collisions at the same energy will also allow one to better understand the impact of the moderate deformation of ^{197}Au in Au + Au collisions. The collisions of another species, e.g., ^{198}Hg + ^{198}Hg ($\beta_2 = -0.11$) would then probe more deeply the nature of the deformation of ^{197}Au, which, being an odd-mass nucleus, has not been directly measured in low-energy experiments. Having additional systems also provides an independent cross-check on the initial state, for example one can set up three relations like Eq. (10) to "triangulate" the consistency of the three deformation values.

---

[3]A few percent difference in ε_2 might arise because the difference in neutron skin effects between ^{96}Zr and ^{96}Ru [64,65], but these effects are much smaller than the influence of nuclear deformation in the UCC region.

In the second step, one can use flow measurements in conjunction with hydrodynamics to map out the evolution of the quadrupole deformation along the chain of stable samarium isotopes. As proposed in Ref. [11], it would be useful to collide three isotopes: ^{144}Sm ($\beta_2 = 0.08$, as spherical as ^{208}Pb), ^{148}Sm ($\beta_2 = 0.18$, triaxial, much like ^{129}Xe and ^{197}Au), and ^{154}Sm ($\beta_2 = 0.32$ well-deformed like ^{238}U). The evolution of the quadrupole deformation can be mapped precisely at RHIC, thus offering a valuable test of nuclear structure knowledge. This scan also enables a search for enhanced octupole correlations, i.e., β_3 values, which are predicted to be present in the region $Z \approx 56$, $N \approx 88$ [53] including the samarium isotopes. The influence of octupole correlations would manifest in high-energy collisions as enhanced v_3, as well as a modified $\rho(v_3^2, [p_T])$ correlator. Evidence of static octupole moments at low energies is rather sparse, and heavy ion collisions might be a more sensitive approach.

In summary, I have studied the parametric dependence of eccentricity ε_n on the quadrupole β_2, octupole β_3, and hexadecapole β_4 deformations of the nucleus in heavy ion collisions. The mean square eccentricities $\langle \varepsilon_n^2 \rangle$ are found to depend linearly on β_n^2 for $n = 2$, 3, and 4. I also find that β_3 contributes significantly to ε_1, and in noncentral collisions the β_4 also contributes to ε_1 and ε_3. In central collisions, there is very little cross contribution between β_2 and ε_3 and between β_3 and ε_2, although in noncentral collisions β_3 (β_2) contributes modestly to ε_2 (ε_3). Since harmonic flow v_n is directly driven by the corresponding eccentricity, $v_n \propto \varepsilon_n$, one expects very similar parametric dependencies between v_n and β_m for both $m = n$ and $m \neq n$. These findings provide a strong motivation to use heavy ion collisions as a precision tool to scan and map out the ground state nuclear deformations and compare with low energy nuclear measurements, not only for the quadrupole deformation, but also for the octupole deformation, whose evidence is quite sparse in nuclear structure physics. The procedure for doing this is presented. One finds that the nonaxial deformations, in particular the triaxiality of quadrupole deformation, do not influence $\langle \varepsilon_n^2 \rangle$, but they can be probed by other observables such as $v_n - [p_T]$ correlation, and possibly higher-order cumulants of v_n and $[p_T]$. The information about the shape of atomic nuclei obtained in heavy-ion collisions is fully complementary to that obtained in nuclear structure experiments. A carefully planned system scan of stable species in the nuclear chart at RHIC, the LHC, and other collider facilities could open a new direction of research in nuclear physics.

APPENDIX A: AN ANALYTICAL ESTIMATE IN HEAD-ON COLLISIONS

I consider a liquid-drop nuclear potential with a sharp surface, $\rho(r, \theta, \phi) = \rho_0$ when $r < R(\theta, \phi)$ and zero otherwise,

and focus on head-on collisions with maximum overlap, i.e., the two nuclei not only have zero impact parameter, but also need to be aligned in a way to ensure that the overlap region contains all the nucleons $N_{\rm part} = 2A$. However, at the end of this section, I also relax the requirement to consider only zero impact parameter, which corresponds more closely to the realistic scenario when the effects of centrality resolution are taken into account. My goal is to establish the simple parametric dependence between $\langle \varepsilon_n^2 \rangle$ and β_m in Eq. (3).

For this discussion, I switch back to using complex spherical harmonics Y_n^m with the normalization condition on the coefficients, $\sum_{m=-n}^{n} |\alpha_{n,m}|^2 = 1$ and $\alpha_{n,m} = \alpha_{n,-m}^*$. I first re-express Eq. (2) as an integral in 3D, using the relation $r_\perp = r \sin\theta$:

$$\varepsilon_n e^{in\Phi_n} = -\frac{\int r^n \sin^n\theta\, e^{in\phi} \rho(\vec{r}) d^3\vec{r}}{\int r^n \sin^n\theta \rho(\vec{r}) d^3\vec{r}} = -\sqrt{\frac{4\pi (2n)!!}{(2n+1)!!}}$$
$$\times \frac{\int (1 + \sum_{l,m} \beta_l \alpha_{l,m} Y_l^m)^{n+3} Y_n^n \sin\theta\, d\theta\, d\phi}{\int (1 + \sum_{l,m} \beta_l \alpha_{l,m} Y_l^m)^{n+3} \sin^{n+1}\theta\, d\theta\, d\phi}, \quad \text{(A1)}$$

where I have used $Y_n^n = \sqrt{\frac{(2n+1)!!}{4\pi (2n)!!}} \sin^n\theta e^{in\phi}$ and the fact that the range of integration along radial direction is $r \in [0, R_0(1 + \sum_{l,m} \beta_l \alpha_{l,m} Y_l^m)]$. Keeping the integration to leading order in β_n, one has

$$\varepsilon_n e^{in\Phi_n} = -A_n \int \left(\sum_{l,m} \beta_l \alpha_{l,m} Y_l^m Y_n^n \right) \sin\theta\, d\theta\, d\phi = -A_n \beta_n \alpha_{n,n},$$

$$A_n \equiv \frac{(n+3)\Gamma(1 + 1/2 + n/2)}{\pi \Gamma(1 + n/2)} \sqrt{\frac{(2n)!!}{(2n+1)!!}}. \quad \text{(A2)}$$

This result is easy to understand: for tip-tip collisions where the z axis is aligned with beam direction (middle row of Fig. 1), only the Y_n^n component can contribute to the eccentricity. The results, $\varepsilon_n = A_n \beta_n / \sqrt{2}$, for a nuclear surface containing only this mode $R = R_0(1 + \beta_n Y_{n,n}) = R_0(1 + \beta_n / \sqrt{2}[Y_n^{-n} + (-1)^n Y_n^n])$, are listed as the first term of each entry in the second row of Table I.

In order to calculate the body-body collision for $Y_{n,0} = Y_n^0$ shown in the top row of Fig. 1, the nuclear surface, or equivalently the direction of projection Y_n^n, needs to be rotated by Euler angles $(\alpha_e, \beta_e, \gamma_e) = (0, \pi/2, 0)$, i.e., $Y_n^n = \sum_{m'} D_{n,m'}^n(0, \pi/2, 0) Y_n^{m'}$, where $D_{n,m'}^n$ is the Wigner rotational matrix. Plugging this into Eq. (A2) and considering only axial deformation $R = R_0(1 + \beta_n Y_n^0)$ give $\varepsilon_n = A_n D_{n,0}^n(0, \pi/2, 0) \beta_n = \sqrt{(2n)!}/(n!2^n) A_n \beta_n$. The values are provided as the first term of each entry in the top row of Table I.

The calculation of Eq. (A1) including higher-order terms in β_n is straightforward, and the full expressions up to the second-order expansion are listed in the table. Interestingly, It is found that if one only considers the expansion for a nuclear surface described by axial deformations $R = R_0(1 + \beta_2 Y_{2,0} + \beta_3 Y_{3,0} + \beta_4 Y_{4,0})$ in the numerator of an equation similar to Eq. (A1), the ratios of the coefficients of the high-order terms to that of the leading order in the first row of Table I are exactly the same as Eq. (13) in Ref. [73]. However, including

also the influence of the denominator of Eq. (A1) modifies the coefficients of some of the second-order terms.

Next, I consider random orientation of the nucleus around its center of mass described by Euler angles $\Omega = (\alpha_e, \beta_e, \gamma_e)$,

and the rotations of the two nuclei are required to be the same. For the purpose to calculating the ε_n, it is equivalent to rotate the transverse plane by applying the substitution $Y_n^n \rightarrow \sum_{m'} D_{n,m'}^n(\alpha, \beta, \gamma) Y_n^{m'}$, in Eq. (A2):

$$\varepsilon_n e^{in\Phi_n} = -A_n \int \left(\sum_{l,m,m'} \beta_l \alpha_{l,m} D_{n,m'}^n Y_l^m Y_n^{m'} \right) \sin\theta \, d\theta \, d\phi = -A_n \left(\sum_{l,m,m'} \beta_l \alpha_{l,m} D_{n,m'}^n \delta_{ln} \delta_{m,-m'} \right) = -A_n \beta_n \sum_m \alpha_{n,m} D_{n,m}^n. \quad (A3)$$

Using the orthogonality relation for the D matrix, the mean square average over Euler angles is

$$\langle \varepsilon_n^2 \rangle = A_n^2 \beta_n^2 \int \left(\sum_m \alpha_{n,m} D_{n,m}^n \right) \left(\sum_{m'} \alpha_{n,m'} D_{n,m'}^n \right)^* \frac{d\Omega}{8\pi^2} = \frac{A_n^2}{2n+1} \beta_n^2. \quad (A4)$$

The result apparently is independent of the mixture of different shape components Y_n^m, as long as the overall magnitude β_n remains the same. The numerical values are listed in the third row of Table I.

The dipolar eccentricity can be calculated in a similar way. The angular weight involved is decomposed into two spherical harmonics, $\sin^3\theta e^{i\phi} = 8/5\sqrt{\pi/21}(Y_3^1 - \sqrt{14}Y_1^1)$, which implies that an octupole nuclear shape can give rise to a dipole eccentricity. As the original nuclear surface has no dipole component, Y_1^1 drops out, and one obtains,

$$\varepsilon_1 e^{i\Phi_1} = -\frac{\int r^3 \sin^3\theta \, e^{i\phi} \rho(\vec{r}) d^3\vec{r}}{\int r^3 \sin^3\theta \, \rho(\vec{r}) d^3\vec{r}} \approx -\frac{64}{5\sqrt{21\pi^3}} \beta_3 \int \sum_m \alpha_{3,m} Y_3^m \left(\sum_{m'} D_{1,m'}^3 Y_3^{m'} \right) = -\frac{64}{5\sqrt{21\pi^3}} \beta_3 \sum_m \alpha_{3,m} D_{1,m}^3. \quad (A5)$$

Therefore the ms average of dipolar eccentricity over all orientations gives

$$\langle \varepsilon_1^2 \rangle = \frac{64^2}{525\pi^3} \beta_3^2 \frac{1}{8\pi^2} \int \sum_{m,m'} \alpha_{3,m} \alpha_{3,m'}^* D_{1,m}^3 D_{1,m}^{3*} d\Omega = \frac{4096}{3625\pi^3} \beta_3^2, \quad (A6)$$

again independently of the mixture of different shape components Y_3^m. Note that this remarkable contribution is present entirely because of the $r_\perp^3$ weight in the definition of ε_1 in Eq. (2), which is naturally required by the cumulant framework [13].

Next, I consider the possible contribution of quadrupole deformation to the ε_4. For this purpose, one expands the nuclear shape in the numerator of Eq. (A1) and, keeping terms that are proportional to β_2^2,

$$\varepsilon_4 \approx 3A_4 \beta_2^2 \int \sum_{m,m'} \alpha_{2,m} \alpha_{2,m'} D_{4,-m-m'}^4 Y_2^m Y_2^{m'} Y_4^{-m-m'} \sin\theta \, d\theta \, d\phi$$

$$= 3A_4 \beta_2^2 \frac{15}{\sqrt{4\pi}} \sum_{m,m'} \alpha_{2,m} \alpha_{2,m'} D_{4,-m-m'}^4 \begin{pmatrix} 2 & 2 & 4 \\ 0 & 0 & 0 \end{pmatrix} \begin{pmatrix} 2 & 2 & 4 \\ m & m' & -m-m' \end{pmatrix} \quad (A7)$$

$$= \frac{45}{2\pi} \sqrt{\frac{2}{35}} \beta_2^2 \left[\alpha_{4,0}' D_{4,0}^4 + \frac{\alpha_{4,2}'}{\sqrt{2}} (D_{4,2}^4 + D_{4,-2}^4) + \frac{\alpha_{4,4}'}{\sqrt{2}} (D_{4,4}^4 + D_{4,-4}^4) \right], \quad (A8)$$

where $\alpha_{4,0}' = [7 + 5\cos(2\gamma)]/12$, $\alpha_{4,2}' = \sqrt{5/12}\sin(2\gamma)$, and $\alpha_{4,4}' = [1 - \cos(2\gamma)]\sqrt{35}/12$, satisfying $(\alpha_{4,0}')^2 + (\alpha_{4,2}')^2 + (\alpha_{4,4}')^2 = 1$. The average over Euler angles gives

$$\langle \varepsilon_4^2 \rangle = \frac{45^2}{4\pi^2} \frac{2}{35} \beta_2^4 \int \left(\sum_m \alpha_{4,m}' D_{4,m}^4 \right) \left(\sum_{m'} \alpha_{4,m'}' D_{4,m'}^4 \right)^* \frac{d\Omega}{8\pi^2} = \frac{45}{14\pi^2} \beta_2^4. \quad (A9)$$

Lastly, I consider the case when one only keeps the zero impact parameter requirement. Ignoring the few nucleons (or a small portion of the volume) that may not be in the overlap region, Eq. (A3) is simply the average of two nuclei with different Euler angles Ω_1 and Ω_2:[4]

$$\varepsilon_n e^{in\Phi_n} = -A_n \frac{\beta_n}{2} \sum_m \alpha_{n,m}[D_{n,m}^n(\Omega_1) + D_{n,m}^n(\Omega_2)]. \quad (A10)$$

From this, the mean square average, similarly to Eq. (A4), needs to be integrated over both Ω_1 and Ω_2. The crossing terms such as $D_{n,m}^n(\Omega_1) D_{n,m}^n(\Omega_2)^*$ vanish after this integration, and the final result is exactly half of the original value. This argument also applies to the $\langle \varepsilon_1^2 \rangle$ in Eq. (A6) and the quadrupole contribution to ε_4 in Eq. (A9). So for a more realistic selection of ultracentral collisions corresponding to close to zero impact parameter, the coefficients of the β_n^2 dependence are a factor of 2 smaller. These values are listed in the bottom row of Table I and they are closer to Monte Carlo Glauber model result shown in the bottom row of Figs. 2 and 3.
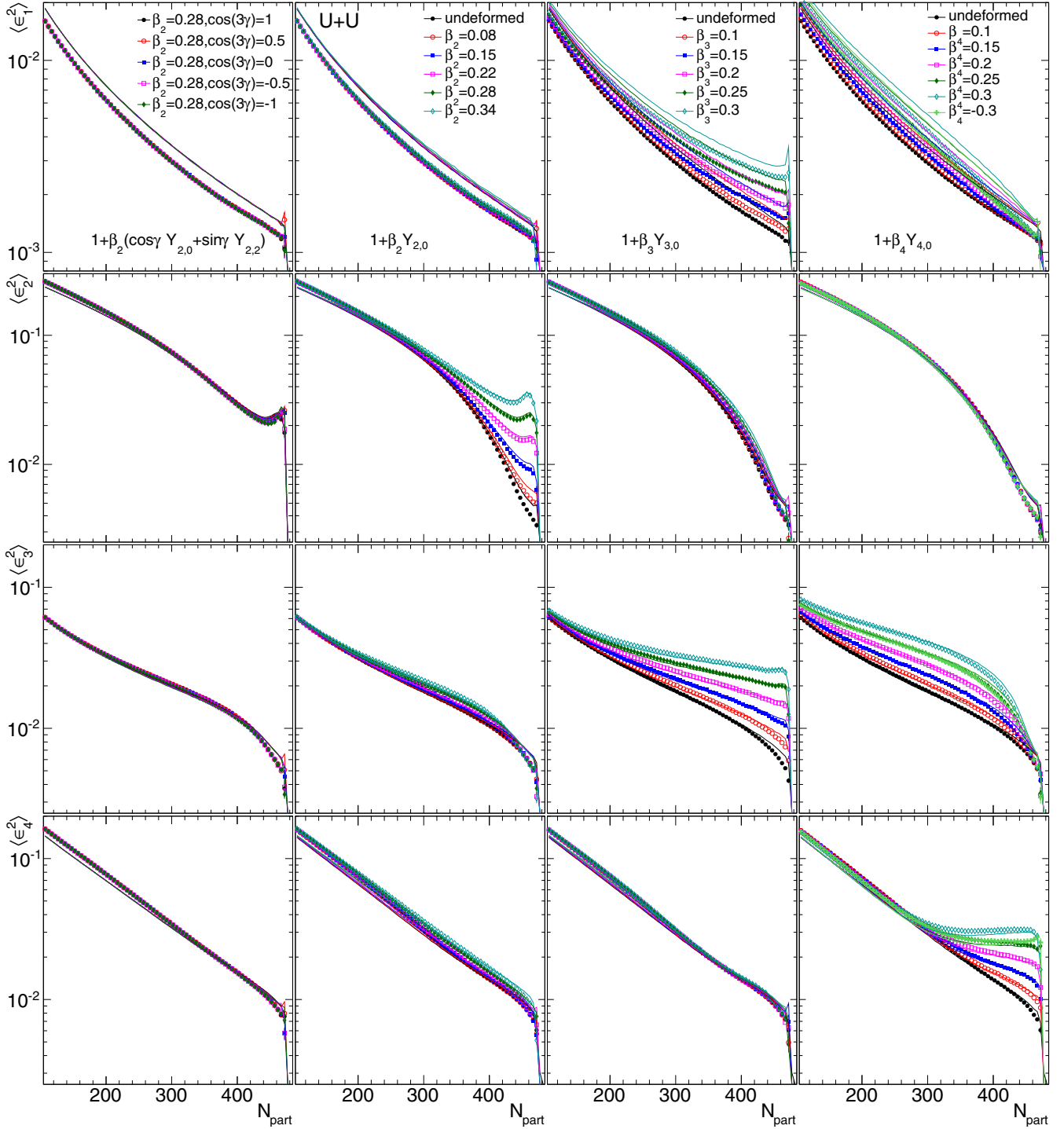
---

[4]I am unable to derive an analytical formula for the contribution of the small portion of volume not included in the overlap region. For a few special cases, not including this volume is found to reduce slightly the coefficients of the β_n^2 dependence.

FIG. 10. The centrality dependence, characterized by N_{part}, of $\langle \varepsilon_n^2 \rangle$ in U + U collisions in the presence of different quadrupole triaxiality γ for $\beta_2 = 0.28$ (left column), different axial quadrupole deformation β_2 (second column), different axial octupole deformation β_3 (third column), and different axial hexadecapole deformation β_4 (last column) for $n = 1$ (top row), $n = 2$ (second row), $n = 3$ (third row), and $n = 4$ (bottom row). The markers and line curves represent $\langle \varepsilon_n^2 \rangle$ calculated from the nucleon Glauber model and quark Glauber model, respectively. The functional form of the deformation and different parameters are given in the top-row panel for each corresponding column.

APPENDIX B: MORE DETAILED RESULTS

For completeness, the full set of correlations between mean square eccentricities $\langle \varepsilon_n^2 \rangle$ and deformation parameters

γ, β_2, β_3, and β_4 in Eq. (1) are included here. The $\langle \varepsilon_n^2 \rangle$ are calculated using the nucleon Glauber model and quark Glauber model in the U + U collisions. They are compiled in Figs. 10 and 11 as a function of two centrality estimators,
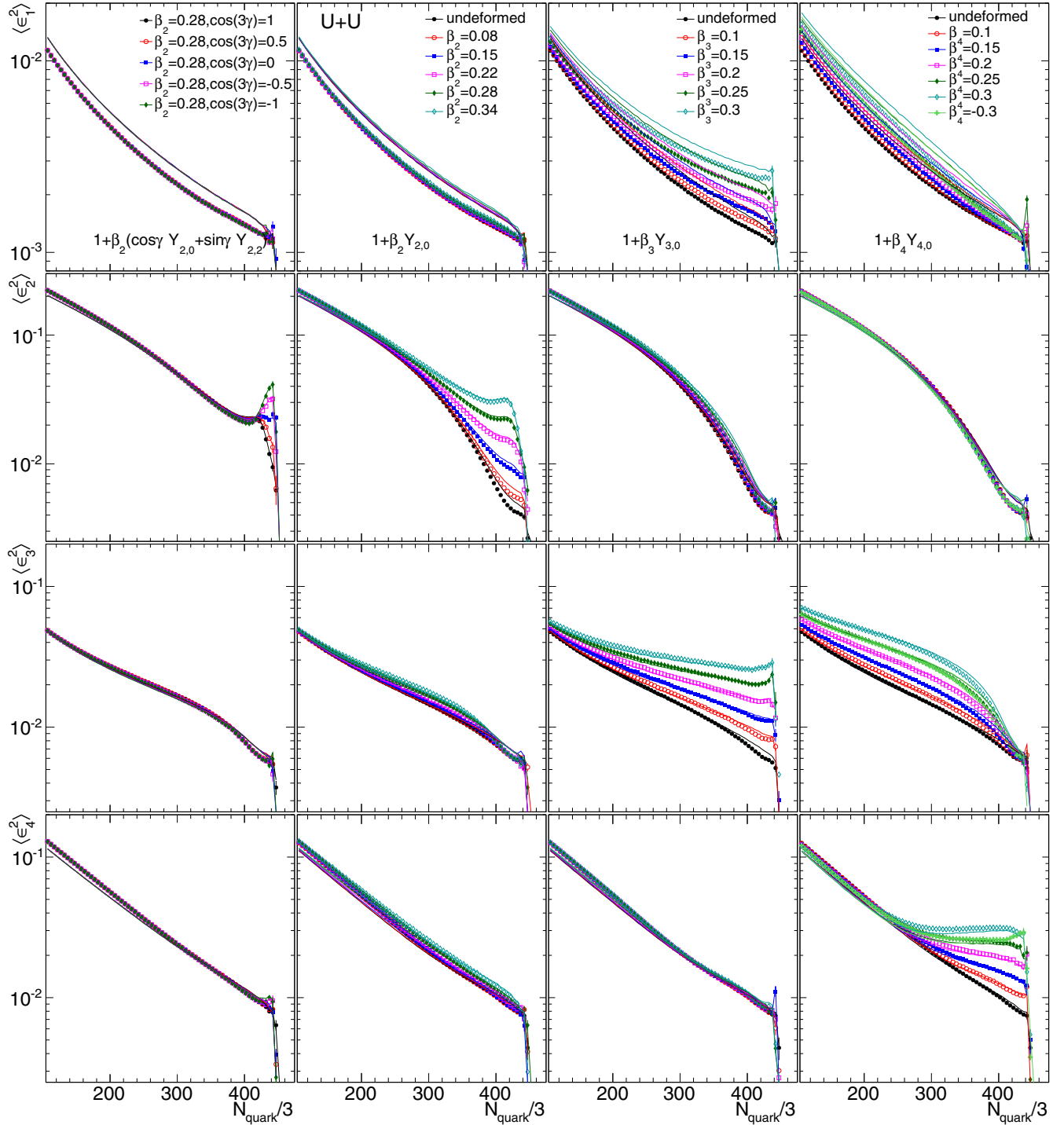
FIG. 11. Same as Fig. 10 but using the N_{quark} as centrality.

N_{part} and N_{quark}, respectively. From these plots, the ratios of $\langle \varepsilon_n^2 \rangle$ to that obtained for default choice of each parameter are plotted in Figs. 12 and 13, respectively. For the smaller $\text{Zr} + \text{Zr}$ collision system, I only show the ratios in Figs. 14 and 15.

The main difference between the two centrality estimators is in the behavior of $\langle \varepsilon_n^2 \rangle$ in the UCC region, more clearly visible in the ratio plots. However, whether $\langle \varepsilon_n^2 \rangle$ themselves

are calculated from nucleons or quarks has little influence on these ratios. Another important point is about the contribution of β_m to $\langle \varepsilon_n^2 \rangle$ for $m \neq n$. Although such mixings could in principle be used to constrain the β_3 using v_1 as well as β_4 using v_1 and v_3, this mixing also forbids a straightforward disentanglement of different deformation components. Fortunately, such mixing effects are minimal in the UCC collisions, and, if one stays in the 0–1% centrality range, each $\langle \varepsilon_n^2 \rangle$
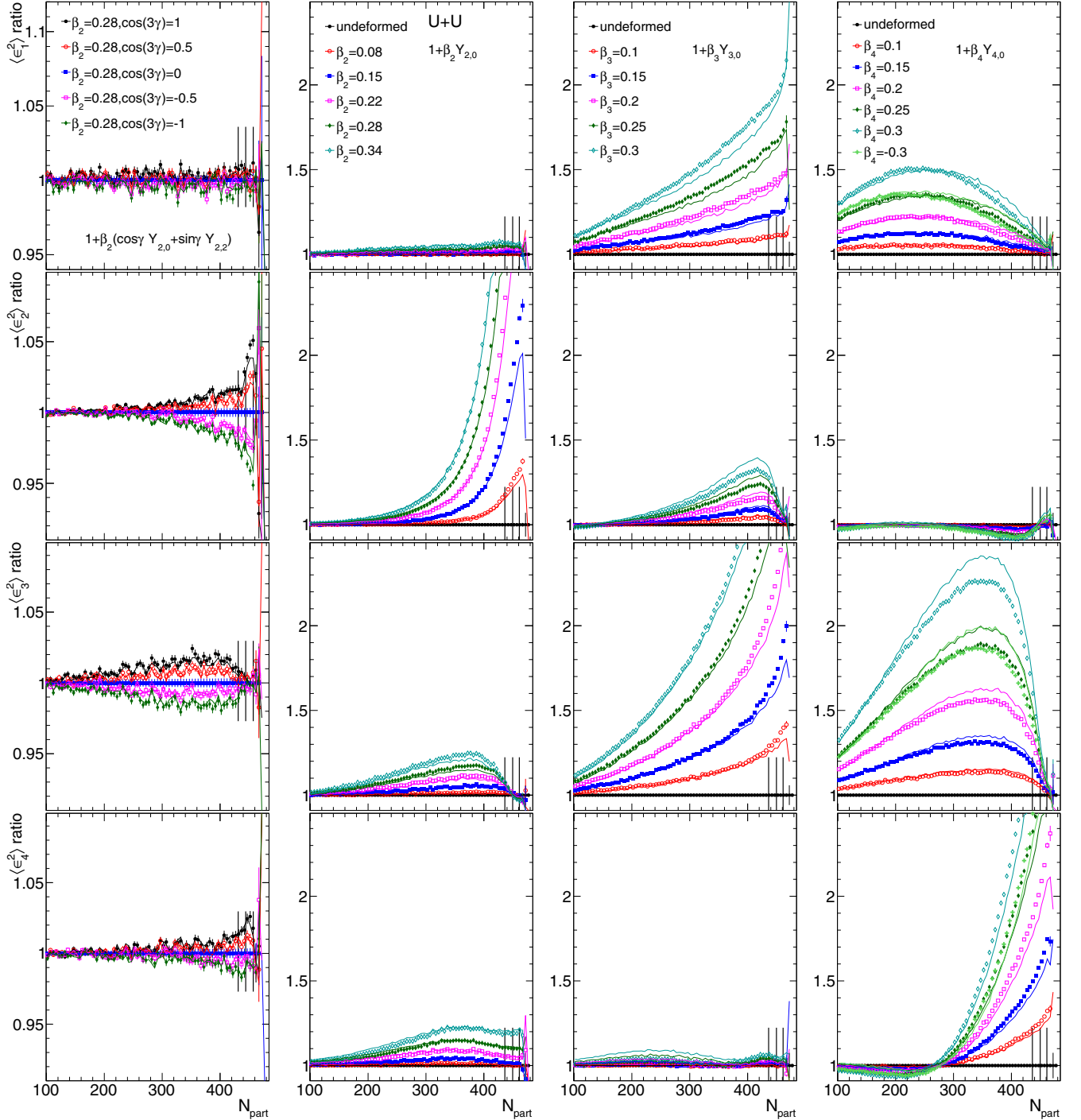
FIG. 12. The ratio of $\langle \varepsilon_n^2 \rangle$ to the $\langle \varepsilon_n^2 \rangle$ in U + U collisions calculated with the default choice of each parameter (indicated by marks or lines around unity in each panel); they are obtained directly from Fig. 10. The three solid vertical bars around unity in each one of these ratio plots indicate the locations of 2%, 1%, and 0.2% centrality.

only has one dominating contribution: $\langle \varepsilon_n^2 \rangle_{\text{UCC}} = a'_n + b'_n \beta_n^2$ for $n = 2, 3,$ and 4 and $\langle \varepsilon_1^2 \rangle_{\text{UCC}} = a'_1 + b'_{3,1} \beta_3^2$. In noncentral collisions, there is a modest cross-correlation between β_3 and $\langle \varepsilon_2^2 \rangle$ and between β_2 and $\langle \varepsilon_3^2 \rangle$, with the former having somewhat larger amplitudes. However, in the medium-size Zr + Zr collision system, the cross correlation between β_3 and

$\langle \varepsilon_2^2 \rangle$ is still significant, but almost disappears between β_2 and $\langle \varepsilon_3^2 \rangle$ (see Figs. 14 and 15). The reason can be explained as follows. In the large U + U collision system, one notes that the maximum influence of β_3 on $\langle \varepsilon_2^2 \rangle$ appears at larger N_{part} or N_{quark} (around 3.5% centrality) than the location of the maximum influence of β_2 on $\langle \varepsilon_3^2 \rangle$ (around 6% centrality). In
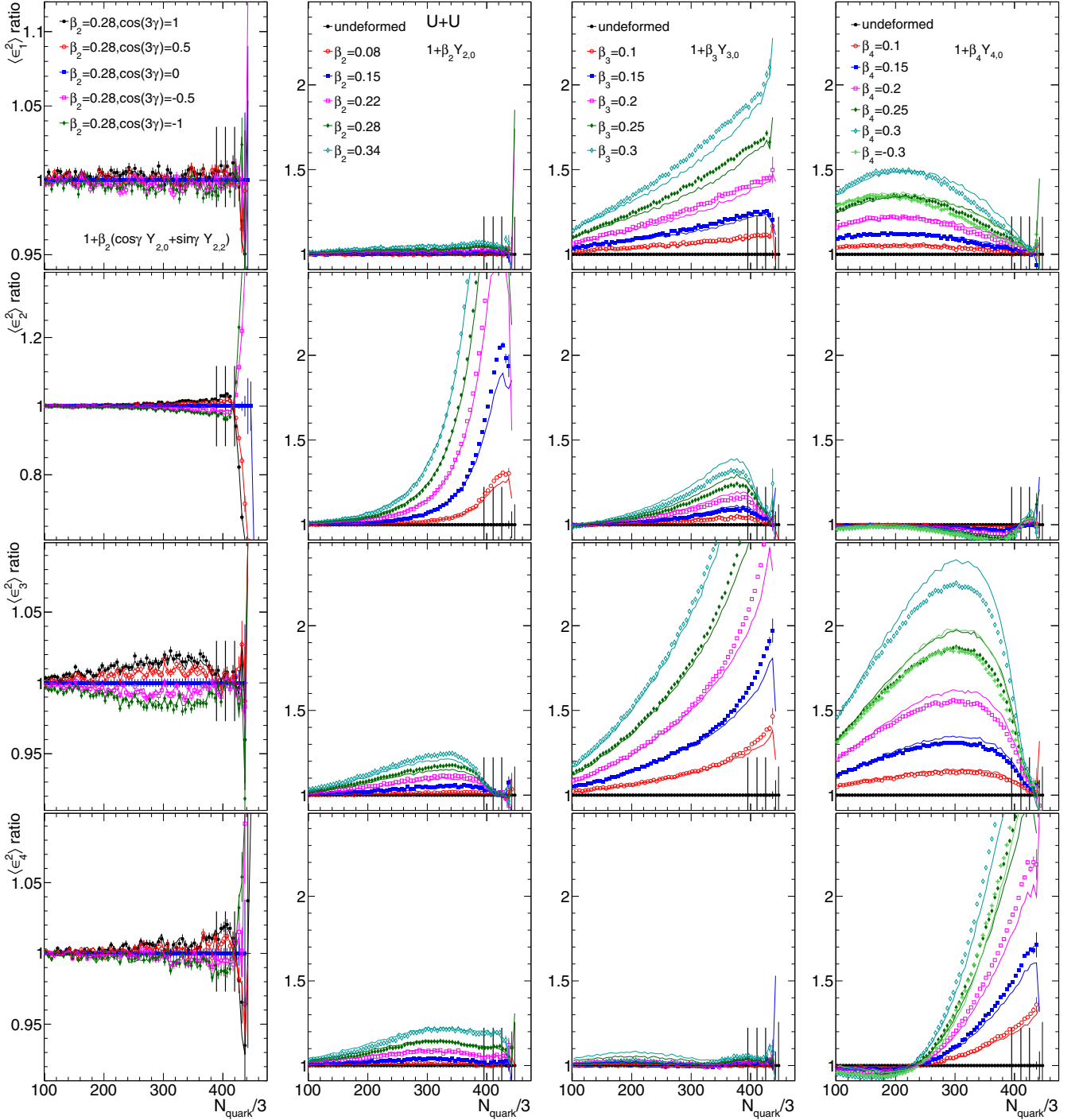
FIG. 13. Same as Fig. 12 but using the N_{quark} as centrality.

the smaller Zr + Zr collision system, the peak location shifts towards the more peripheral region, maximum influence of β_3 on $\langle\varepsilon_2^2\rangle$ shifts to around 7% centrality, and the maximum influence of β_3 on $\langle\varepsilon_2^2\rangle$ shifts to around 15% centrality. In the latter case, the fluctuation-driven $\langle\varepsilon_3^2\rangle$ component is much more important than enhancement from β_2. In the former case, the $\langle\varepsilon_2^2\rangle$ value for the undeformed case is also larger, leading

to a smaller relative increase compared to U + U for the same β_3.

Focusing on the 0–1% centrality range, I then obtain the $\langle\varepsilon_n^2\rangle$ as a function of various β_n^2. The results are summarized in Figs. 16 and 17 for U + U and Zr + Zr collisions, respectively. In most cases, strict linear dependencies are observed. One noticeable exception is the relation between $\langle\varepsilon_4^2\rangle$ and
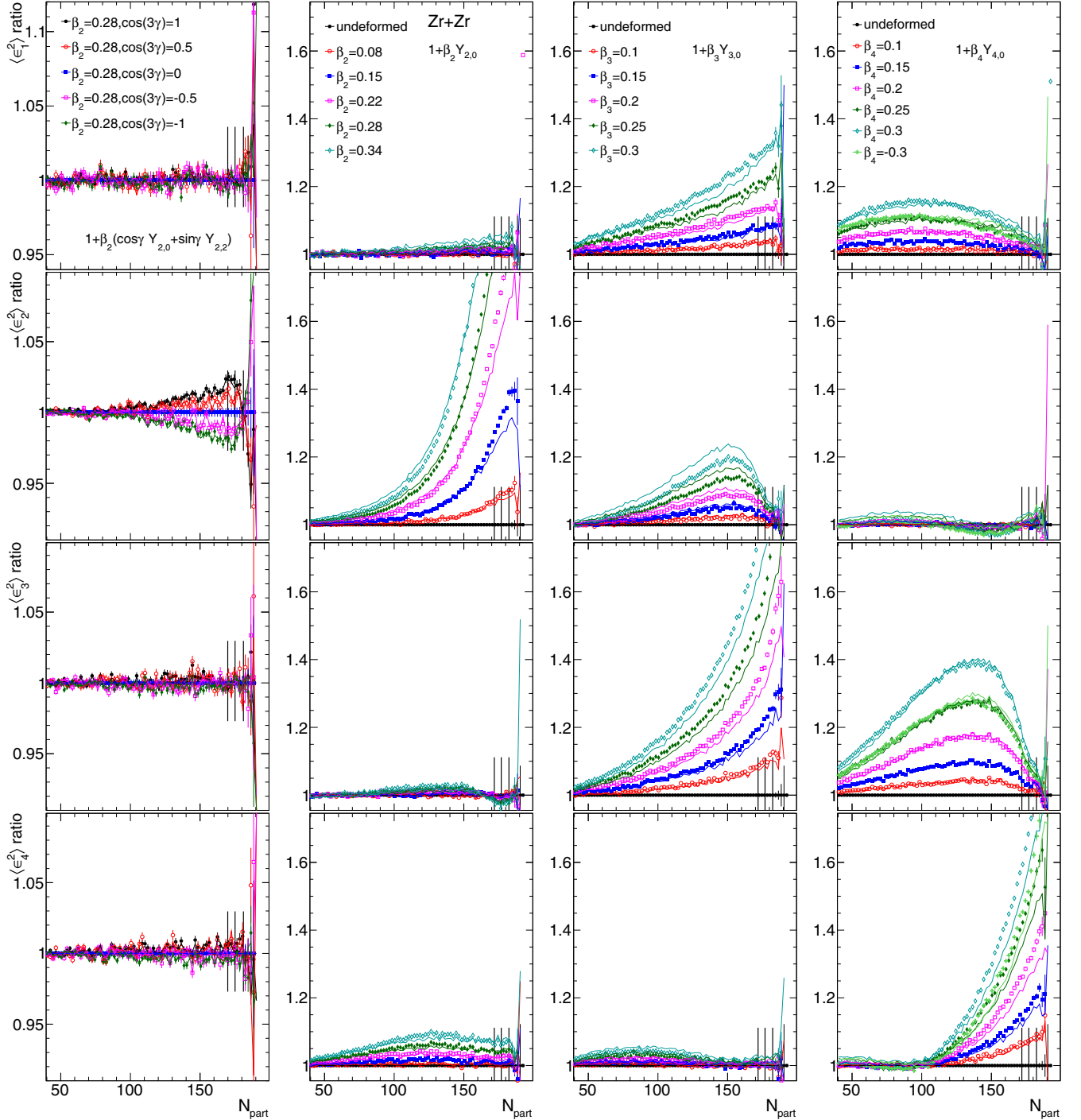
FIG. 14. Same as Fig. 12 but for Zr + Zr collisions.

β_2, which is better described by a quartic dependence β_2^4 in the UCC region of U + U, consistent with the analytical results in Table I. However, in the mid-central and peripheral U + U collisions and in Zr + Zr over the full centrality range, one finds that it is still better described by a β_2^2 dependence. Lastly, the slopes of these dependencies are nearly independent of whether nucleons or quarks are used for ε_n

or the centrality, with the exception of the γ dependence of $\langle \varepsilon_2^2 \rangle$.

Section III B discusses briefly the influence of nonaxial higher-order deformation, analogous to the triaxiality for the quadrupole deformation. This aspect is explored by mixing two different octupole or hexadecapole components, while keeping the overall magnitude of the deformation
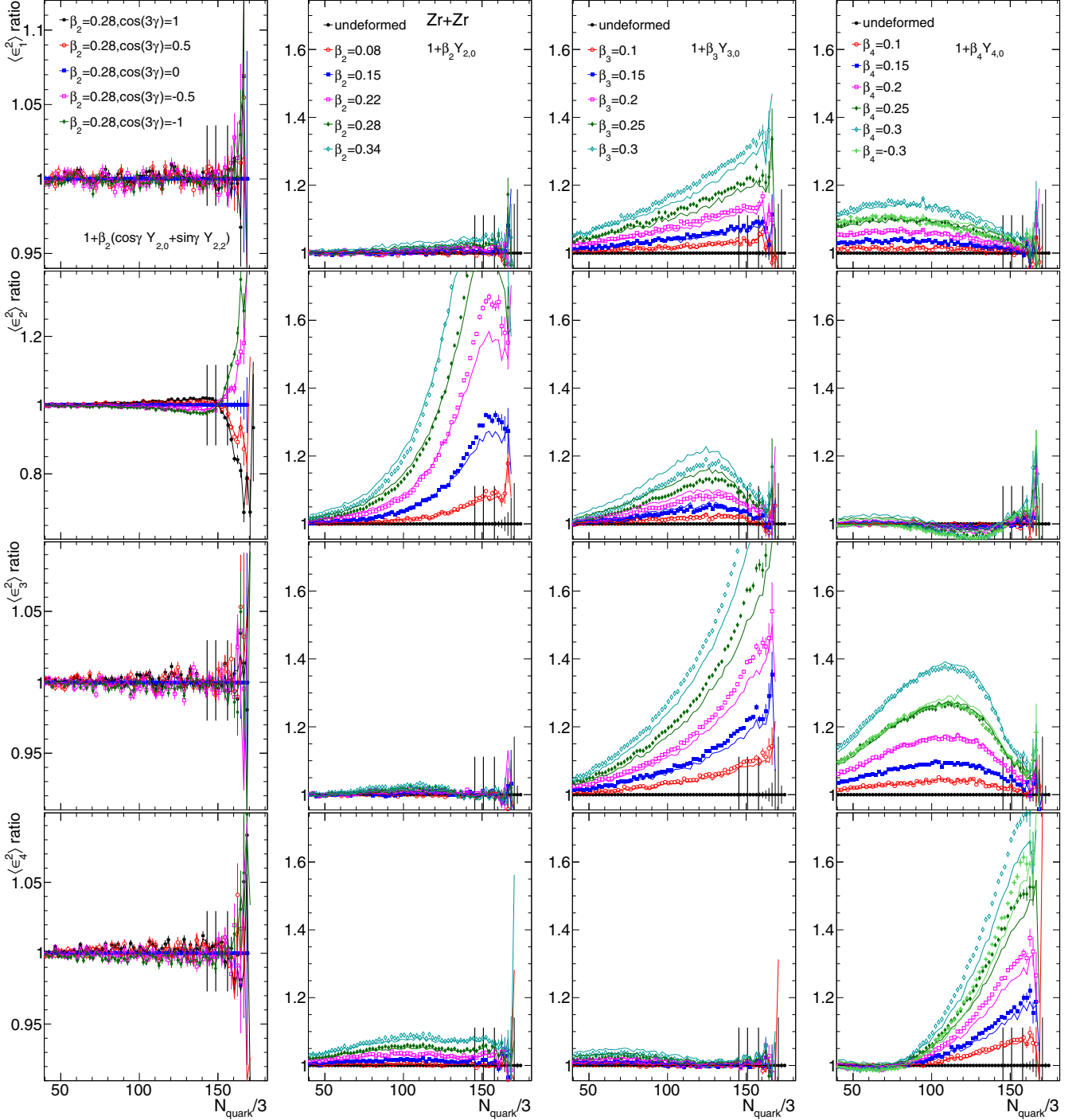
FIG. 15. Same as Fig. 13 but for Zr + Zr collisions.

the same. Three cases are studied for the octupole deformation, $1 + \beta_3(\cos \delta Y_{3,0} + \sin \delta Y_{3,1})$, $1 + \beta_3(\cos \delta Y_{3,0} + \sin \delta Y_{3,2})$, and $1 + \beta_3(\cos \delta Y_{3,0} + \sin \delta Y_{3,3})$; the results are shown in the left three columns of Fig. 18. Only a small, less than 3%, dependence on the mixing angle δ is observed for $\langle \varepsilon_3^2 \rangle$. The situation for hexadecapole is a bit more involved. To simplify the discussion, I consider only the components respecting all three reflection symmetries, $Y_{4,0}$, $Y_{4,2}$, and $Y_{4,4}$.

The nuclear surface can be parametrized with two angular variables γ_4 and δ_4, in addition to β_4 [51,74]:

$$R(\theta, \phi) = R_0(1 + \beta_4\{\cos \delta_4 Z_0 + \sin \delta_4[\cos \gamma_4 Z_1 + \sin \gamma_4 Z_2]\}),$$

$$Z_0 = \sqrt{\frac{7}{12}} Y_{4,0} + \sqrt{\frac{5}{12}} Y_{4,4},$$

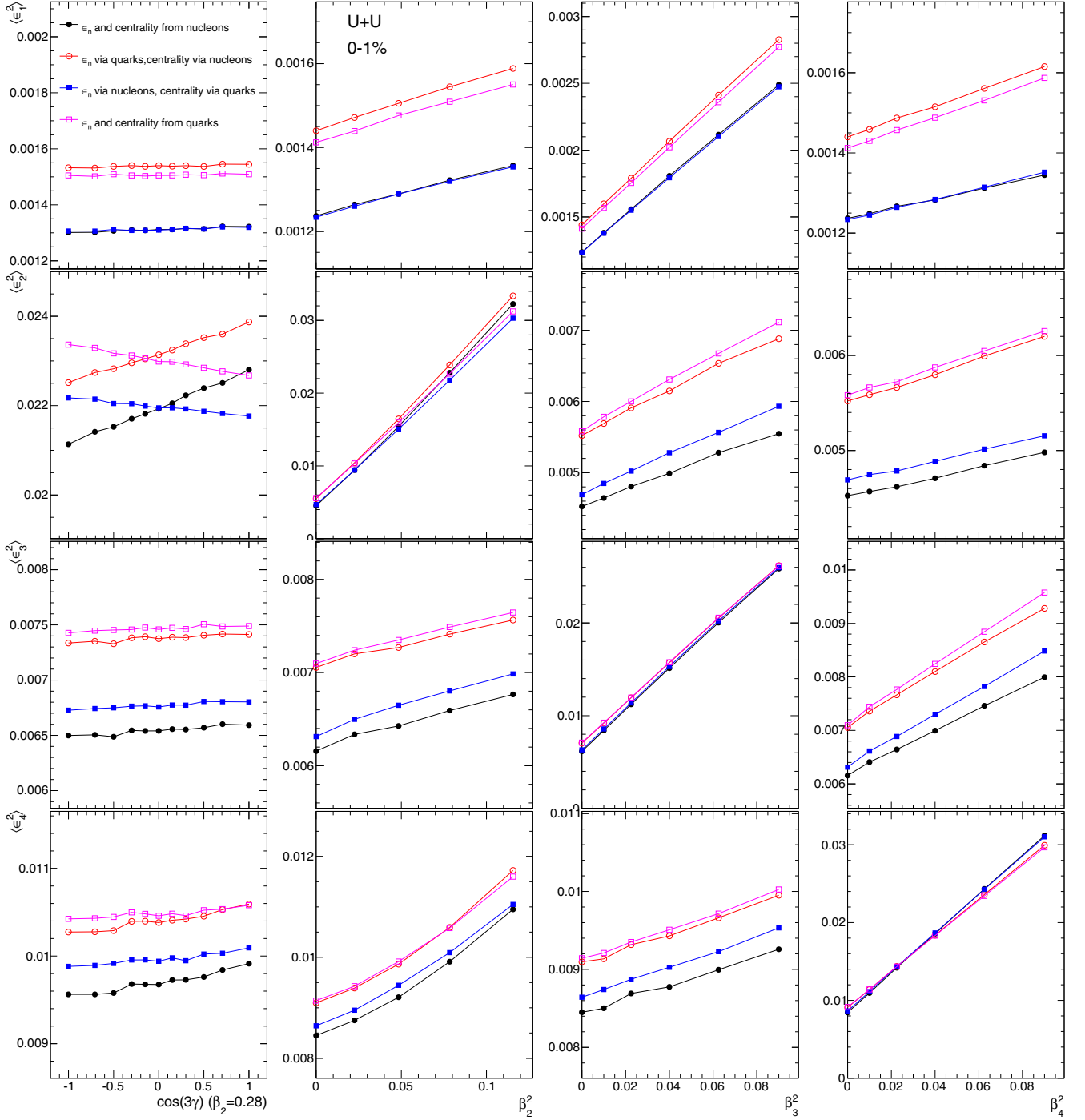$$Z_1 = \sqrt{\frac{5}{12}} Y_{4,0} - \sqrt{\frac{7}{12}} Y_{4,4}, \quad Z_2 = Y_{4,2}. \quad (\text{B1})$$

FIG. 16. The parametric dependence of $\langle \varepsilon_n^2 \rangle$ in 0–1% centrality U + U collisions on the quadrupole triaxiality γ for $\beta_2 = 0.28$ (left column), axial quadrupole deformation β_2 (second column), axial octupole deformation β_3 (third column), and axial hexadecapole deformation β_4 (last column) for $n = 1$ (top row), $n = 2$ (second row), $n = 3$ (third row), and $n = 4$ (bottom row). The $\langle \varepsilon_n^2 \rangle$ and centrality can be determined from either the nucleon Glauber or quark Glauber, model leading to four different curves in each panel as indicated by the legend in the top-left panel. They are obtained directly from plots like Figs. 10 and 11, where each panel provides the two set of data points in the corresponding panel in this figure.

The parameter γ_4 plays a role similar to the triaxiality parameter γ. For example, for $\delta_4 = \mathrm{acos}(\sqrt{7/12})$, $\gamma_4 = 0$, $2\pi/3$, and $4\pi/3$ would correspond to axial-hexadecapole

shape around z, x, and y axes, respectively. The right two columns of Fig. 18 show results for the two mixing cases, $1 + \beta_4(\cos\gamma_4 Z_1 + \sin\gamma_4 Z_2)$ and $1 + \beta_4(\cos\delta_4 Z_0 + \sin\delta_4 Z_1)$,
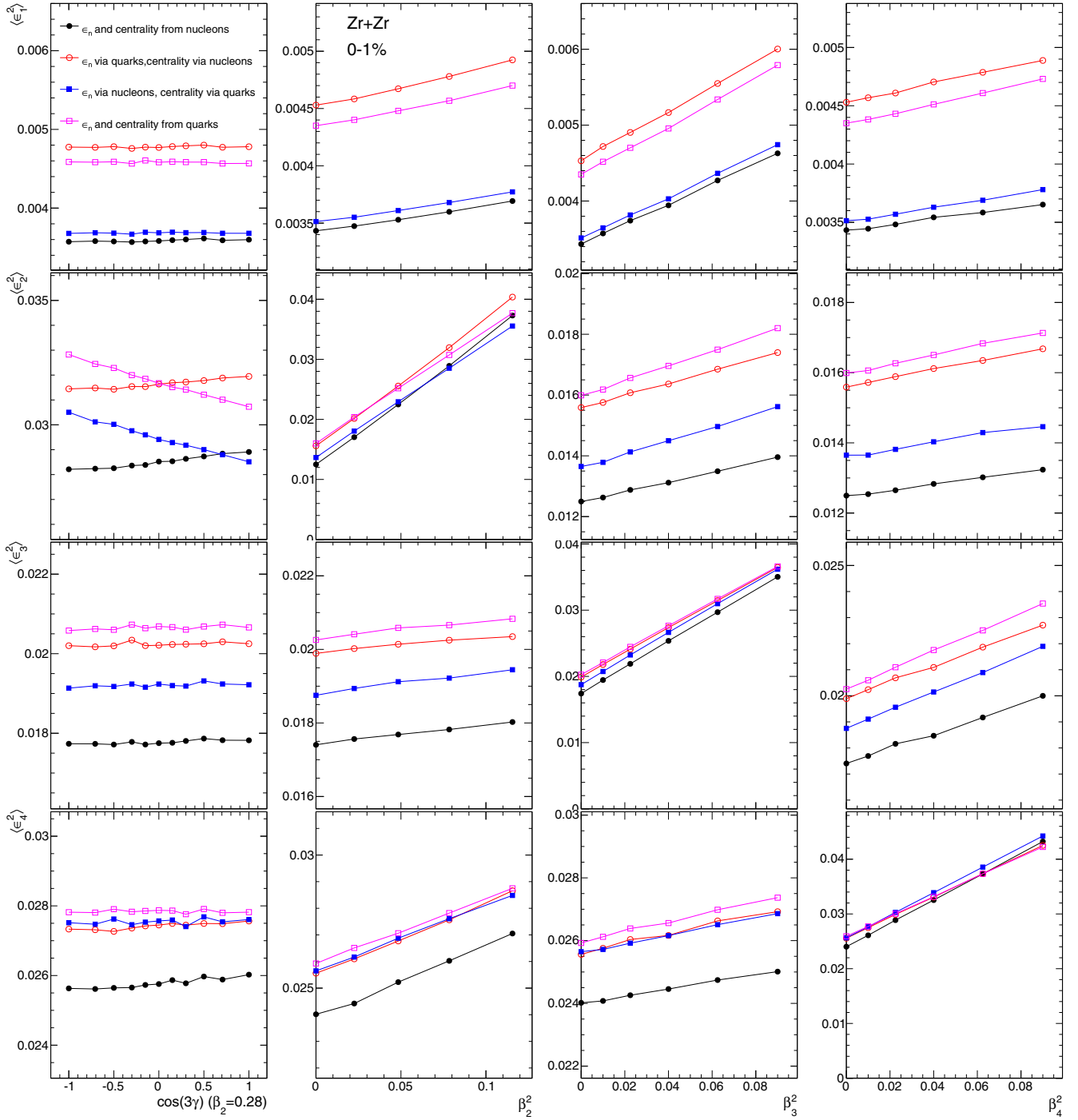
FIG. 17. Same as Fig. 16 but for 0–1% most central Zr + Zr collisions.

respectively. A clear linear dependence on $\cos 3\gamma_4$ is observed in the first case. The dependence in the second case is somewhat more complex, but I do observe it reaches maximum when $\delta_4 = 0$ or $\pi/2$, for which hexadecapole shape is described by $Z_0 = \sqrt{\frac{7}{12}}Y_{4,0} + \sqrt{\frac{5}{12}}Y_{4,4}$ or $Z_1 = \sqrt{\frac{5}{12}}Y_{4,0} -$

$\sqrt{\frac{7}{12}}Y_{4,4}$ and positive $\beta_4 = |\beta_4|$. The minimum on the other hand corresponds to the same shape components but with $\beta_4 = -|\beta_4|$. This behavior is similar to the influence the prolate vs oblate quadrupole deformation on the $\langle \varepsilon_2^2 \rangle$ as seen in Fig. 4.
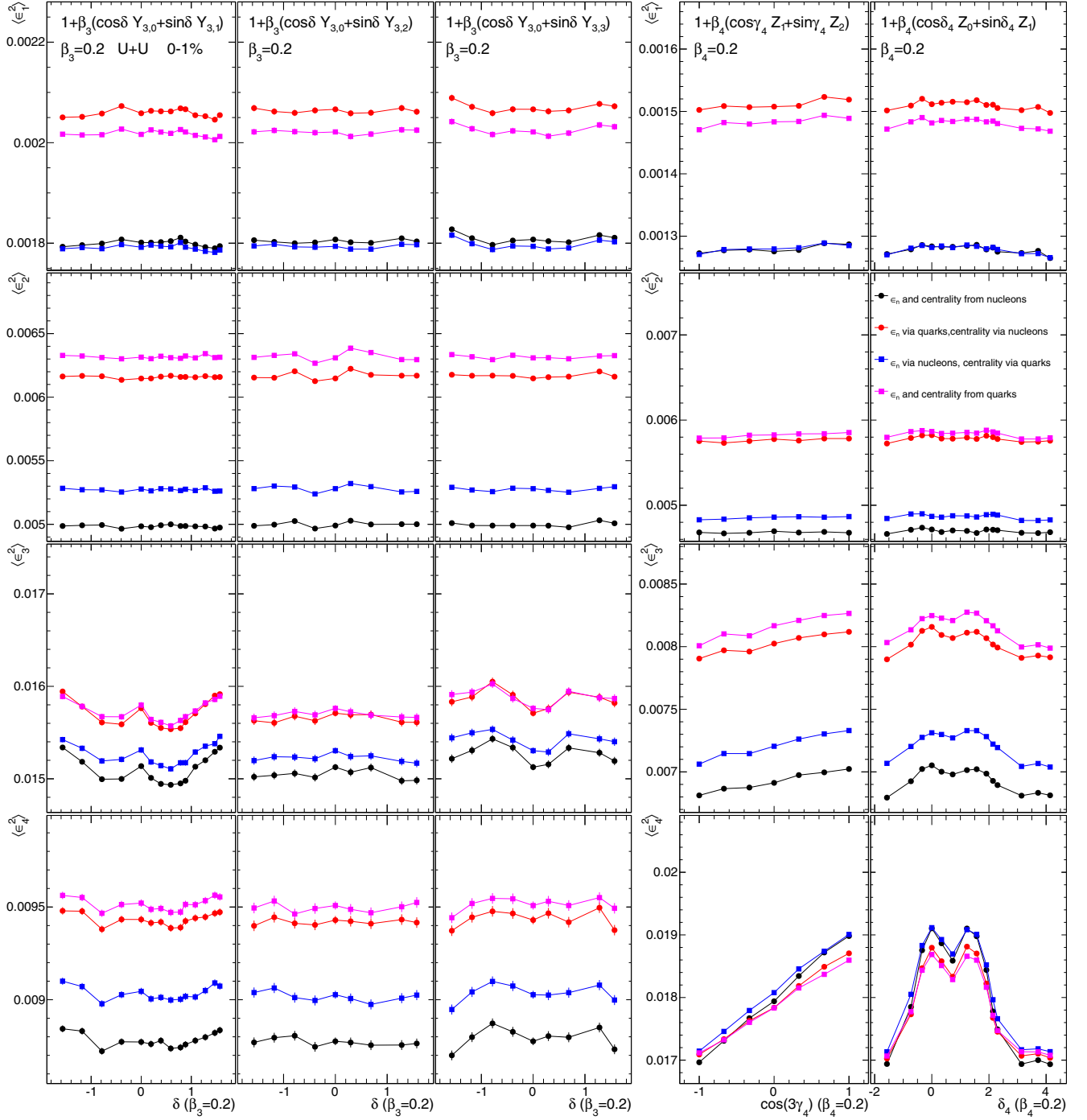
FIG. 18. Effects of mixing between three pairs of octupole components in the left three columns, $1 + \beta_3(\cos \delta Y_{3,0} + \sin \delta Y_{3,1})$, $1 + \beta_3(\cos \delta Y_{3,0} + \sin \delta Y_{3,2})$, and $1 + \beta_3(\cos \delta Y_{3,0} + \sin \delta Y_{3,3})$, and between two pairs of hexadecapole components in the right two columns, $1 + \beta_4(\cos \gamma_4 Z_1 + \sin \gamma_4 Z_2)$ and $1 + \beta_4(\cos \delta_4 Z_0 + \sin \delta_4 Z_1)$, where $Z_0 = \sqrt{\frac{7}{12}}Y_{4,0} + \sqrt{\frac{5}{12}}Y_{4,4}$, $Z_1 = \sqrt{\frac{5}{12}}Y_{4,0} - \sqrt{\frac{7}{12}}Y_{4,4}$, and $Z_2 = Y_{4,2}$ (see text). The results are obtained for 0–1% central U + U collisions and are presented separately for $\langle \varepsilon_n^2 \rangle$, $n = 1$, 2, 3, and 4 from the top to the bottom rows. The $\langle \varepsilon_n^2 \rangle$ and centrality are determined from either a nucleon Glauber or quark Glauber model, leading to four different curves in each panel as indicated by the legend in the right panel of the second row.

[1] *Nuclear Structure*, edited by A. Bohr and B. R. Mottelson (World Scientific, Singoapore, 1998).

[2] K. Heyde and J. L. Wood, Rev. Mod. Phys. **83**, 1467 (2011).

[3] T. Togashi, Y. Tsunoda, T. Otsuka, and N. Shimizu, Phys. Rev. Lett. **117**, 172502 (2016).

[4] K. Heyde and J. L. Wood, Phys. Scr. **91**, 083008 (2016).

[5] S. Frauendorf, Phys. Scr. **93**, 043003 (2018).

[6] S.-G. Zhou, Phys. Scr. **91**, 063008 (2016).

[7] H. De Vries, C. W. De Jager, and C. De Vries, At. Data Nucl. Data Tables **36**, 495 (1987).

[8] W. Busza, K. Rajagopal, and W. van der Schee, Annu. Rev. Nucl. Part. Sci. **68**, 339 (2018).

[9] U. W. Heinz, J. Phys.: Conf. Ser. **455**, 012044 (2013).

[10] T. Nakatsukasa, K. Matsuyanagi, M. Matsuo, and K. Yabana, Rev. Mod. Phys. **88**, 045004 (2016).

[11] G. Giacalone, J. Jia, and C. Zhang, Phys. Rev. Lett. **127**, 242301 (2021).

[12] C. G. Joslin and C. Gray, Mol. Phys. **50**, 329 (1983).

[13] D. Teaney and L. Yan, Phys. Rev. C **83**, 064904 (2011).

[14] H. Niemi, K. J. Eskola, and R. Paatelainen, Phys. Rev. C **93**, 024907 (2016).

[15] D. Teaney and L. Yan, Phys. Rev. C **86**, 044908 (2012).

[16] J. Jia, J. Phys. G **41**, 124003 (2014).

[17] J. E. Bernhard, J. S. Moreland, S. A. Bass, J. Liu, and U. Heinz, Phys. Rev. C **94**, 024907 (2016).

[18] J. E. Bernhard, J. S. Moreland, and S. A. Bass, Nat. Phys. **15**, 1113 (2019).

[19] G. Nijs, W. van der Schee, U. Gürsoy, and R. Snellings, Phys. Rev. Lett. **126**, 202301 (2021).

[20] A. Rosenhauer, H. Stocker, J. A. Maruhn, and W. Greiner, Phys. Rev. C **34**, 185 (1986).

[21] B.-A. Li, Phys. Rev. C **61**, 021903(R) (2000).

[22] S. Das Gupta and C. Gale, Phys. Rev. C **62**, 031901(R) (2000).

[23] U. W. Heinz and A. Kuhlman, Phys. Rev. Lett. **94**, 132301 (2005).

[24] P. Filip, R. Lednicky, H. Masui, and N. Xu, Phys. Rev. C **80**, 054903 (2009).

[25] Q. Y. Shou, Y. G. Ma, P. Sorensen, A. H. Tang, F. Videbæk, and H. Wang, Phys. Lett. B **749**, 215 (2015).

[26] A. Goldschmidt, Z. Qiu, C. Shen, and U. Heinz, Phys. Rev. C **92**, 044903 (2015).

[27] G. Giacalone, J. Noronha-Hostler, M. Luzum, and J.-Y. Ollitrault, Phys. Rev. C **97**, 034904 (2018).

[28] G. Giacalone, Phys. Rev. C **99**, 024910 (2019).

[29] L. Adamczyk et al. (STAR Collaboration), Phys. Rev. Lett. **115**, 222301 (2015).

[30] S. Acharya et al. (ALICE Collaboration), Phys. Lett. B **784**, 82 (2018).

[31] A. M. Sirunyan et al. (CMS Collaboration), Phys. Rev. C **100**, 044902 (2019).

[32] G. Aad et al. (ATLAS Collaboration), Phys. Rev. C **101**, 024906 (2020).

[33] P. Carzon, S. Rao, M. Luzum, M. Sievert, and J. Noronha-Hostler, Phys. Rev. C **102**, 054905 (2020).

[34] G. Giacalone, Phys. Rev. Lett. **124**, 202301 (2020).

[35] G. Giacalone, Phys. Rev. C **102**, 024901 (2020).

[36] J. Jia, S. Huang, and C. Zhang, arXiv:2105.05713 (to be published).

[37] J. Jia, Nuclear deformation effects via Au+Au and U+U collisions from STAR, contribution to the VIth International Conference on the Initial Stages of High-Energy Nuclear Collisions, January 2021 (unpublished), https://indico.cern.ch/event/854124/contributions/4135480/.

[38] M. L. Miller, K. Reygers, S. J. Sanders, and P. Steinberg, Annu. Rev. Nucl. Part. Sci. **57**, 205 (2007).

[39] S. S. Adler et al. (PHENIX Collaboration), Phys. Rev. C **89**, 044905 (2014).

[40] R. A. Lacey, P. Liu, N. Magdy, M. Csanád, B. Schweid, N. N. Ajitanand, J. Alexander, and R. Pak, Universe **4**, 22 (2018).

[41] C. Loizides, Phys. Rev. C **94**, 024914 (2016).

[42] P. Bożek, W. Broniowski, and M. Rybczyński, Phys. Rev. C **94**, 014902 (2016).

[43] S. Acharya et al. (ALICE Collaboration), Phys. Lett. B **790**, 35 (2019).

[44] M. Zhou and J. Jia, Phys. Rev. C **98**, 044903 (2018).

[45] J. T. Mitchell, D. V. Perepelitsa, M. J. Tannenbaum, and P. W. Stankus, Phys. Rev. C **93**, 054910 (2016).

[46] T. De Forest, Jr. and J. D. Walecka, Adv. Phys. **15**, 1 (1966).

[47] W. D. Myers and K.-H. Schmidt, Nucl. Phys. A **410**, 61 (1983).

[48] A. Mazeliauskas and D. Teaney, Phys. Rev. C **91**, 044902 (2015).

[49] A. Mazeliauskas and D. Teaney, Phys. Rev. C **93**, 024913 (2016).

[50] I. Hamamoto, X.-Z. Zhang, and H.-X. Xie, Phys. Lett. B **257**, 1 (1991); **278**, 511(E) (1992).

[51] S. G. Rohozinski, Phys. Rev. C **56**, 165 (1997).

[52] R. C. Lemmon, J. R. Leigh, J. X. Wei, C. R. Morton, D. J. Hinde, J. O. Newton, J. C. Mein, M. Dasgupta, and N. Rowley, Phys. Lett. B **316**, 32 (1993).

[53] P. A. Butler, J. Phys. G **43**, 073002 (2016).

[54] G. L. P et al., Nature (London) **497**, 199 (2013).

[55] W. Nazarewicz, P. Olanders, I. Ragnarsson, J. Dudek, G. A. Leander, P. Möller, and E. Ruchowsa, Nucl. Phys. A **429**, 269 (1984).

[56] S. Raman, C. W. G. Nestor, Jr., and P. Tikkanen, At. Data Nucl. Data Tabl. **78**, 1 (2001).

[57] S. E. Agbemava, A. V. Afanasjev, and P. Ring, Phys. Rev. C **93**, 044304 (2016).

[58] J. Libert, M. Meyer, and P. Quentin, Phys. Rev. C **25**, 586 (1982).

[59] P. Möller, A. J. Sierk, T. Ichikawa, and H. Sagawa, At. Data Nucl. Data Tabl. **109-110**, 1 (2016).

[60] L. M. Robledo and G. F. Bertsch, Phys. Rev. C **84**, 054302 (2011).

[61] S. Hilaire and M. Girod, Eur. Phys. J. A **33**, 237 (2007).

[62] T. Kibédi and R. H. Spear, At. Data Nucl. Data Tabl. **80**, 35 (2002).

[63] G. Giacalone, J. Jia, and V. Somà, Phys. Rev. C **104**, L041903 (2021).

[64] J. Hammelmann, A. Soto-Ontoso, M. Alvioli, H. Elfner, and M. Strikman, Phys. Rev. C **101**, 061901(R) (2020).

[65] H.-j. Xu, H. Li, X. Wang, C. Shen, and F. Wang, Phys. Lett. B **819**, 136453 (2021).

[66] P. Huo, J. Jia, and S. Mohapatra, Phys. Rev. C **90**, 024910 (2014).

[67] B. H. Alver, C. Gombeaud, M. Luzum, and J.-Y. Ollitrault, Phys. Rev. C **82**, 034913 (2010).

[68] R. S. Bhalerao, M. Luzum, and J.-Y. Ollitrault, Phys. Rev. C **84**, 054901 (2011).

[69] S. S. Gubser and A. Yarom, Nucl. Phys. B **846**, 469 (2011).

[70] P. Staig and E. Shuryak, Phys. Rev. C **84**, 034908 (2011).

[71] R. A. Lacey, D. Reynolds, A. Taranenko, N. N. Ajitanand, J. M. Alexander, F.-H. Liu, Y. Gu, and A. Mwai, J. Phys. G **43**, 10LT01 (2016).

[72] F. G. Gardim and J.-Y. Ollitrault, Phys. Rev. C **103**, 044907 (2021).

[73] W. Ryssens, M. Bender, K. Bennaceur, P. H. Heenen, and J. Meyer, Phys. Rev. C **99**, 044315 (2019).

[74] P. Magierski, K. Burzynski, E. Perlinska, J. Dobaczewski, and W. Nazarewicz, Phys. Rev. C **55**, 1236 (1997).